

Chapter 2

Single Pulse Voltammetry: Reversible Electrochemical Reactions

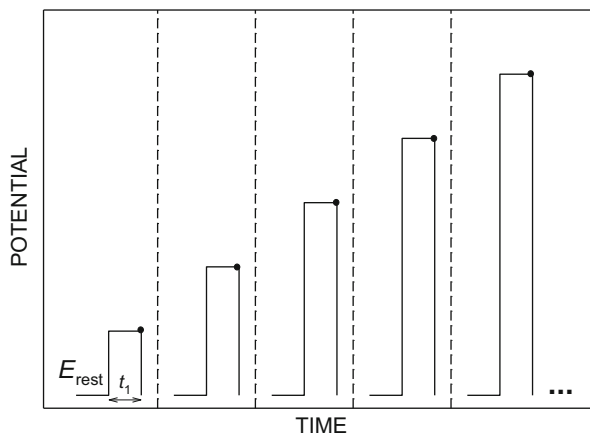
Contents

2.1	Introduction	67
2.1.1	Reversible Electrode Reaction	69
2.2	Planar Electrodes	69
2.2.1	Concentration Profiles	72
2.2.2	Current–Time Curves (Chronoamperometry) and Current–Potential Curves (Voltammetry)	74
2.2.3	Stoichiometric Coefficients Different From the Unity	79
2.3	Ion Transfer Through Liquid Membranes	81
2.3.1	One-Polarized Interface Systems	82
2.3.2	Two-Polarized Interfaces Systems	84
2.3.3	Electron Transfer at the Liquid/Liquid Interface	90
2.4	Dropping Mercury Electrode (DME)	94
2.4.1	dc Polarography	96
2.4.2	Normal Pulse Polarography (NPP)	99
2.5	Spherical Electrodes	101
2.5.1	Unequal Diffusion Coefficients ($D_O \neq D_R$)	103
2.5.2	Equal Diffusion Coefficients ($D_O = D_R$)	108
2.6	Other Electrodes Geometries	111
2.7	Microelectrodes. Steady-State Voltammetry	120
2.8	Rotating Disc Electrode	123
2.9	Thin Layer Voltammetry	126
	References	129

2.1 Introduction

In a single potential step voltammetric technique, several constant potentials (of increasing amplitude) are applied with a time length t_1 . When stationary electrodes are used, the time interval between two consecutive potentials must be much greater than t_1 for the initial conditions to be restored (Scheme 2.1). If a Static Mercury Drop Electrode (SMDE) is used, the initial conditions are simply restored by making the drop fall. The measured current at a fixed time value $t = t_1$ is plotted discretely versus the corresponding potential steps [1–3]. The resulting current–potential curve has a sigmoidal shape whose position and slope depend on the

Scheme 2.1 Potential–time waveform for Single Potential Pulse Voltammetry. E_{rest} is a potential at which no faradaic processes take place at the electrode. *Black dots* indicate the times at which the current is sampled and *vertical dashed lines* correspond to the recovery of the initial equilibrium conditions



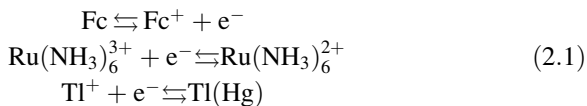
reversibility of the electrode process and the wave height is independent of the electron transfer rate. At each fixed potential value, the current–time variation (which has a typical cottrellian behavior for reversible processes at planar electrodes when considering diffusive transport only) can be registered. If the length time is in the range 2–200 ms, the electrochemical technique is called Normal Pulse Voltammetry (NPV), originally known as Normal Pulse Polarography (NPP). This technique was introduced by Barker [5–7] and it was originally designed for the Dropping Mercury Electrode (DME), in which the potential pulse is applied at the end of the life of the drop, with the current being dependent on the relation between the pulse time and the drop lifetime. The main reason for measuring the current at the end of short time intervals is to eliminate the capacitive component (see Sect. 1.9) in order to optimize the sensitivity. Today the DME electrode is scarcely used and most electrochemical techniques are used at stationary electrodes

A complete comprehension of Single Pulse electrochemical techniques is fundamental for the study of more complex techniques that will be analyzed in the following chapters. Hence, the concept of “half-wave potential,” for example, will be defined here and then characterized in all electrochemical techniques [1, 3, 8]. Moreover, when very small electrodes are used, a stationary current–potential response is reached. This is independent of the conditions of the system prior to each potential step and even of the way the current–potential was obtained (i.e., by means of a controlled potential technique or a controlled current one) [9, 10]. So, the stationary solutions deduced in this chapter for the current–potential curves for single potential step techniques are applicable to any multipotential step or sweep technique such as Staircase Voltammetry or Cyclic Voltammetry. Moreover, many of the functional dependences shown in this chapter for different diffusion fields are maintained in the following chapters when multipulse techniques are described if the superposition principle can be applied.

2.1.1 Reversible Electrode Reaction

For an electrode reaction to be considered reversible, it is necessary to compare the rate of the charge transfer process and the rate of the mass transport of electroactive species. When the mass transport rate is slower than the charge transfer one, the electrode reaction is controlled by the transport rate and can be considered as electrochemically reversible in that the surface concentration fulfills the Nernst equation when a given potential is applied to the electrode. In Electrochemistry, knowledge of the behavior of reversible electrode processes is very important, since these can be used as a benchmark for more complex systems (see Chap. 5 in [1] and Sect. 1.8.4 for a detailed discussion).

There are many examples of reversible (or nernstian) behavior.¹ For example, the redox conversions of a great number of metallic complexes such as Ferrocene, $\text{Ru}(\text{NH}_3)_6^{3+}$, or metallic cations like Tl^+ (see Eq. (2.1) for the redox reactions in detail²). It is important to highlight that the reversible behavior can also be obtained in many cases by acting on suitable experimental parameters in the particular electrochemical technique used. Under the appropriate experimental conditions, the characterization of these types of processes can be applied to many systems.



2.2 Planar Electrodes

From a practical point of view, a macroelectrode can be considered as an electrode whose characteristic dimension L is much greater than the diffusion layer thickness (i.e., in general $L \gg \sqrt{Dt}$, with D being the diffusion coefficient of the electroactive species). For such an electrode, the geometry becomes irrelevant and it can be considered as an infinite planar electrode for which, if the solution contains a great amount of supporting electrolyte, the mass transport is governed by semi-infinite linear diffusion (i.e., it can be assumed that mass transport occurs only in the dimension x normal to the electrode surface) [11]. For this reason, throughout this book, macroelectrodes will be referred as “planar electrodes.”

We consider an electrochemical reversible reaction



¹ An electrochemical reaction is called “reversible” or nernstian when the Nernst’s equation can be applied to the surface concentrations of electroactive species for any value of the applied potential (see Sect. 1.7).

² The reduction of Tl^+ takes place at a mercury electrode so the metals are amalgamated into the electrode.

The calculation of the concentration profiles of species O and R ($c_O(x, t)$ and $c_R(x, t)$) and of the current when a potential E is applied requires solving of the following diffusion equations:

$$\left. \begin{aligned} \frac{\partial c_O}{\partial t} &= D_O \frac{\partial^2 c_O}{\partial x^2} \\ \frac{\partial c_R}{\partial t} &= D_R \frac{\partial^2 c_R}{\partial x^2} \end{aligned} \right\} \quad (2.2)$$

where D_i is the diffusion coefficient of species i ($= O, R$).

The boundary value problem (bvp) is

$$\left. \begin{aligned} t > 0, \quad x \rightarrow \infty \\ t = 0, \quad x \geq 0 \end{aligned} \right\} \quad c_O = c_O^*, \quad c_R = c_R^* \quad (2.3)$$

with c_O^* and c_R^* being the bulk concentrations of species O and R.

The initial condition ($t = 0$) expresses the homogeneity of the solution at the beginning of the experiment, and the semi-infinite condition ($x \rightarrow \infty$) implies that the potential perturbation is not effective far from the electrode.

When the experiment begins, at the electrode surface ($t > 0, x = 0$) the flux balance implies

$$D_O \left(\frac{\partial c_O}{\partial x} \right)_{x=0} = -D_R \left(\frac{\partial c_R}{\partial x} \right)_{x=0} \quad (2.4)$$

Moreover, if nernstian behavior for the charge transfer reaction is assumed, the following condition holds:

$$c_O^{s,r} = e^{\eta} c_R^{s,r} \quad (2.5)$$

with

$$\eta = \frac{F}{RT} (E - E_c^{\ominus'}) \quad (2.6)$$

and $c_O^{s,r}$ and $c_R^{s,r}$ are the surface concentrations of species O and R, i.e., the values of the concentration profiles at $x = 0$. Superscript “r” denotes that the electrochemical reaction is reversible. $E_c^{\ominus'}$ is the formal potential of the redox couple O/R (see Sect. 1.5.1).

The current, according to Faraday law and Fick’s first law, is given by

$$I^{\text{plane}} = FAD_O \left(\frac{\partial c_O}{\partial x} \right)_{x=0} = -FAD_R \left(\frac{\partial c_R}{\partial x} \right)_{x=0} \quad (2.7)$$

This problem can be easily solved by introducing the new variable,

$$s_i^p = \frac{x}{2\sqrt{D_i t}} \quad i = O, R \quad (2.8)$$

where superscript “p” denotes that the parameter s corresponds to planar diffusion.

By introducing s_i^p parameter into Eq. (2.2), Fick’s second law takes the form:

$$\frac{d^2 c_i}{d(s_i^p)^2} + 2s_i^p \frac{dc_i}{ds_i^p} = 0 \quad i = O, R \quad (2.9)$$

and the boundary value problem (Eqs. 2.3–2.5) becomes

$$s_i^p \rightarrow \infty :$$

$$c_i = c_i^* \quad i = O, R \quad (2.10)$$

$$s_i^p = 0 :$$

$$\sqrt{D_O} \left(\frac{dc_O}{ds_O^p} \right)_{s_O^p=0} = -\sqrt{D_R} \left(\frac{dc_R}{ds_R^p} \right)_{s_R^p=0} \quad (2.11)$$

$$c_O(s_O^p = 0) = e^\eta c_R(s_R^p = 0) \quad (2.12)$$

Equation (2.11) refers to the flux conservation and Eq. (2.12) to the establishment of the nernstian equilibrium. Note that under these conditions, the original problem in terms of variables x and t has been transformed into a one-variable problem (s_i^p), that is, c_O and c_R can be expressed only as functions of the variables s_O^p and s_R^p , respectively (which include distance and time variables), because they diffuse with different diffusion coefficients D_O and D_R . This problem can now be solved by making $y_i = dc_i/ds_i^p$, and Eq. (2.9) becomes

$$\frac{dy_i}{ds_i} + 2s_i^p y_i = 0 \quad i = O, R \quad (2.13)$$

whose direct integration leads to

$$y_i = y_i(0) e^{-(s_i^p)^2} \quad (2.14)$$

or,

$$\left(\frac{dc_i}{ds_i^p} \right) = \left(\frac{dc_i}{ds_i^p} \right)_{s_i^p=0} e^{-(s_i^p)^2} \quad (2.15)$$

By integrating (2.15), one obtains

$$c_i(s_i^p) = c_i(s_i^p = 0) + \left(\frac{dc_i}{ds_i^p} \right)_{s_i^p=0} \frac{\sqrt{\pi}}{2} \operatorname{erf}(s_i^p) \quad i = O, R \quad (2.16)$$

By introducing condition (2.10) in Eq. (2.16), it can be deduced for $s_i^p \rightarrow \infty$ that

$$\left(\frac{dc_i}{ds_i^p} \right)_{s_i^p=0} = \frac{2}{\sqrt{\pi}} (c_i^* - c_i(s_i^p = 0)) \quad (2.17)$$

So, Eq. (2.16) becomes

$$c_i(s_i^p) = c_i(s_i^p = 0) + (c_i^* - c_i(s_i^p = 0)) \operatorname{erf}(s_i^p) \quad (2.18)$$

which can be written more conveniently as

$$\left. \begin{aligned} c_O(x, t) &= c_O(s_O^p) = c_O^* + (c_O(s_O^p = 0) - c_O^*) \operatorname{erfc}(s_O^p) \\ c_R(x, t) &= c_R(s_R^p) = c_R^* + (c_R(s_R^p = 0) - c_R^*) \operatorname{erfc}(s_R^p) \end{aligned} \right\} \quad (2.19)$$

with $\operatorname{erf}(z)$ being the Error function of “ z ” given by $\operatorname{erf}(z) = 2/\sqrt{\pi} \int_0^z e^{-u^2} du$, and $\operatorname{erfc}(z) = 1 - \operatorname{erf}(z)$.

From Eqs. (2.11), (2.12), and (2.17), the surface concentrations $c_O(s_O^p = 0) = c_O^{s,r}$ and $c_R(s_R^p = 0) = c_R^{s,r}$ are obtained,

$$\left. \begin{aligned} c_O^{s,r} &= \frac{e^\eta (\gamma c_O^* + c_R^*)}{1 + \gamma e^\eta} \\ c_R^{s,r} &= \frac{\gamma c_O^* + c_R^*}{1 + \gamma e^\eta} \end{aligned} \right\} \quad (2.20)$$

with

$$\gamma = \sqrt{\frac{D_O}{D_R}} \quad (2.21)$$

From Eq. (2.20), it is fulfilled that

$$\sqrt{D_O} c_O^{s,r} + \sqrt{D_R} c_R^{s,r} = \sqrt{D_O} c_O^* + \sqrt{D_R} c_R^* \quad (2.22)$$

2.2.1 Concentration Profiles

Equations (2.19) show the concentration profiles for species O and R. The linear concentration profiles of these species correspond to the lines tangent to $c_i(x, t)$ at the electrode surface (i.e., at $x = 0$) and are given by

$$c_i(x, t) = \frac{c_i^* - c_i^{s,r}}{\delta_{p,i}^r} x + c_i^{s,r} \quad i = O, R \quad (2.23)$$

From Eqs. (2.4), (2.8), (2.17), and (2.19),

$$\left(\frac{\partial c_i}{\partial x} \right)_{x=0} = \left(\frac{dc_i}{ds_i^p} \right)_{s_i^p=0} \left(\frac{\partial s_i^p}{\partial x} \right)_{x=0} = \frac{c_i^* - c_i^{s,r}}{\sqrt{\pi D_i t}} \quad i = O, R \quad (2.24)$$

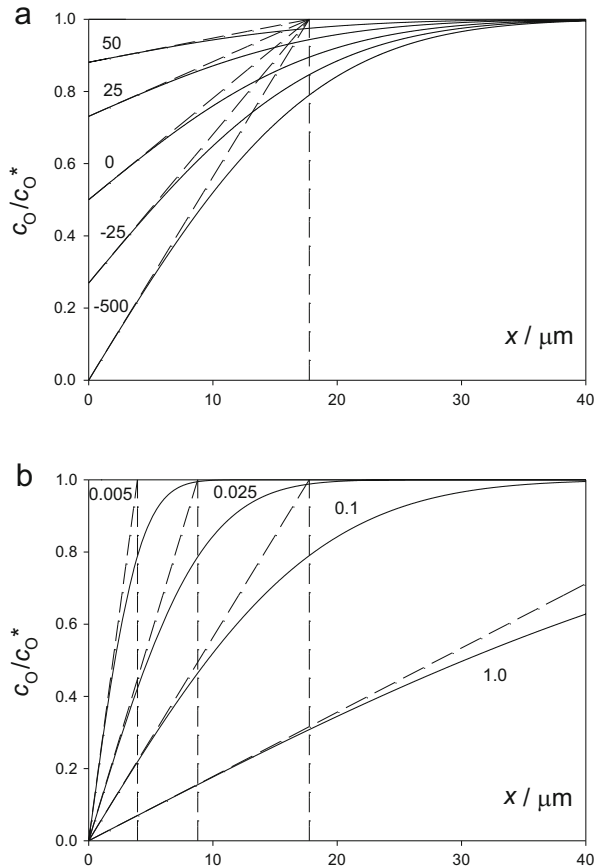
Hence, by comparing Eqs. (2.23) and (2.24) it can be deduced that Nernst diffusion layer for a planar electrode, $\delta_{p,i}^r$, is defined as

$$\delta_{p,i}^r = \sqrt{\pi D_i t} \quad (2.25)$$

In Fig. 2.1, we have plotted the transient accurate concentration profiles for species O, $c_O(x, t)$ (Eq. 2.19), and the linear concentration profiles (Eq. (2.23)) at a

Fig. 2.1 Concentration profiles of species O at a planar electrode calculated from Eq. (2.19) for the application of a potential pulse for different values of $(E - E_c^{\ominus'})$ (in mV) for a fixed time (a), and different values of time (in s) for a fixed potential (b), shown in the curves. *Dashed lines* correspond to their linear concentration profiles.

$t = 0.1$ s (a) and $E - E_c^{\ominus'} = -500$ mV (b). Reproduced with permission [12]



fixed time and different potential values (Fig. 2.1a), and at a fixed potential and different times (Fig. 2.1b).

From Fig. 2.1a, it can be observed that the Nernst diffusion layer, defined by the abscissa at which the concentration reaches the value c_O^* in the linear concentration profile, is independent of the potential in all the cases in spite of their having been obtained under transient conditions. This is in agreement with Eqs. (2.20) and (2.25), which show that the dependence on the electrode potential is only in the surface concentrations.

Figure 2.1b shows the time dependence of the concentration profiles. It can also be observed that the perturbed region of the solution adjacent to the electrode surface grows with time and the relative difference between the linear diffusion layer and the accurate diffusion layer (determined as the value x for which c_O reaches the 99 % of its bulk value) is greater for shorter times [12].

2.2.2 Current–Time Curves (Chronoamperometry) and Current–Potential Curves (Voltammetry)

By inserting Eq. (2.24) in (2.7), the following expression for the current is obtained:

$$I^{\text{plane}} = FAD_O \frac{(c_O^* - c_O^{s,r})}{\sqrt{\pi D_O t}} = -FAD_R \frac{(c_R^* - c_R^{s,r})}{\sqrt{\pi D_R t}} \quad (2.26)$$

By taking into account Eq. (2.20), the current given by (2.26) becomes

$$I^{\text{plane}} = FA \sqrt{\frac{D_O}{\pi t}} \frac{(c_O^* - c_R^* e^\eta)}{1 + \gamma e^\eta} \quad (2.27)$$

with η given by Eq. (2.6).

Note that the reversible $I(E, t)$ response is expressed as a product of a potential-dependent function $((c_O^* - c_R^* e^\eta)/(1 + \gamma e^\eta))$ and a time-dependent function $(FA \sqrt{D_O/(\pi t)})$. This behavior is characteristic of reversible electrode processes. In the next sections the current–time curves at fixed potential (Chronoamperograms) and current–potential curves at a fixed time (Voltammograms) will be analyzed.

2.2.2.1 Chronoamperometry

Expressions for the cathodic and anodic diffusion-controlled limiting currents, $I_{d,c}^{\text{plane}}$ and $I_{d,a}^{\text{plane}}$, can be easily obtained from Eq. (2.27) by making $e^\eta \rightarrow 0$ and $e^\eta \rightarrow \infty$ (i.e., $E \ll E_c^{\ominus'}$ and $E \gg E_c^{\ominus'}$), respectively. For a simple charge transfer the diffusion-controlled limiting current can also be defined as the current at which the electrode reaction is forced by the applied potential to the point that the surface

concentrations of electroactive reactant species fall to zero and then the current is only limited by the diffusion transport. Hence, $I_{d,c}^{\text{plane}}$ and $I_{d,a}^{\text{plane}}$ can also be obtained by making $c_O^{s,r} = 0$ and $c_R^{s,r} = 0$, respectively, in Eq. (2.26),

$$\left. \begin{aligned} I_{d,c}^{\text{plane}} &= FA \sqrt{\frac{D_O}{\pi t}} c_O^* \\ I_{d,a}^{\text{plane}} &= -FA \sqrt{\frac{D_R}{\pi t}} c_R^* \end{aligned} \right\} \quad (2.28)$$

These two equations are known as the Cottrell equations [13]. Equations (2.27) and (2.28) show that the current decays with the square root of time for any value of the applied potential, which only acts as a scale factor, as illustrated in Fig. 2.2. These equations predict very high current at short times, although in practice, the measured current at very short times is influenced both by the intrinsic limitations of the potentiostat and by the cell time constant, with the time needed for the fulfillment of Eqs. (2.27) and (2.28) being higher than $R_u C_{dl}$ (with R_u and C_{dl} being the uncompensated resistance of the cell and the double-layer capacitance; see Sects. 1.6 and 1.9). For sufficiently longer times, deviations from the cottrellian behavior are expected because of the natural convection, that is, the movement of the solution due to density differences, and edge effects, due to nonlinear diffusion at the electrode border.

The measurement of limiting currents is probably the simplest and most widely applicable method for measuring the diffusion coefficients of redox species. In agreement with Cottrell's equation, the value of D_i can be obtained from the plot of

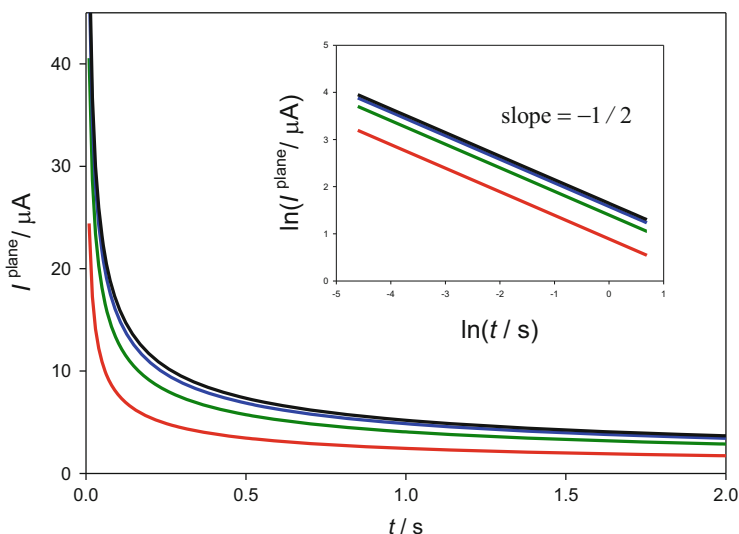


Fig. 2.2 Current–time curves for the application of a constant potential to a planar electrode. $D_O = D_R = 10^{-5} \text{ cm}^2 \text{ s}^{-1}$, $c_O^* = c_R^* = 1 \text{ mM}$, $A = 0.031 \text{ cm}^2$, $T = 298 \text{ K}$. The values of $(E - E_c^{\oplus'})$ in mV are: red, -25 ; green, -50 ; blue, -75 ; black, -100 . The inner figure corresponds to the plot of the logarithm of the current versus the logarithm of time

the logarithm of the limiting current versus the logarithm of time (see inner black curve in Fig. 2.2), by using the relation

$$D_i = \frac{\pi e^{2 \times \text{intercept}}}{(F A c_i^*)^2} \quad (2.29)$$

Additionally, a slope equal to $\frac{1}{2}$ confirms the validity of Eq. (2.28). Note that the Cottrell equation considers planar diffusion as the sole form of mass transport. However, in practice, purely planar diffusion is only achieved with very large or shielding electrodes. Deviations from cottrellian behavior at short times (double-layer current) and long times (convection,³ edge effects⁴) would restrict the applicability of the above equation (see Fig. 2.3).

2.2.2.2 Voltammetry

At a fixed time, the current–potential curve obtained from several potential step experiments has the sigmoidal shape shown in Fig. 2.4. This curve shows some interesting points:

- The potential corresponding to a current $I^{\text{plane}} = (I_{d,c}^{\text{plane}} + I_{d,a}^{\text{plane}})/2$, is called “reversible half-wave potential,” $E_{1/2}^r$, in planar geometry. This parameter can deviate from the formal potential because it is affected by the diffusion coefficients of the electroactive couple and also by the electrode geometry and size (i.e., it is affected by the kinetics of the mass transport); see Fig. 2.21.

To find this point, it is necessary to combine Eqs. (2.26) and (2.28),

$$\left. \begin{aligned} \frac{c_{\text{O}}^{s,r}}{c_{\text{O}}^*} &= 1 - \frac{I^{\text{plane}}}{I_{d,c}^{\text{plane}}} \\ \frac{c_{\text{R}}^{s,r}}{c_{\text{R}}^*} &= 1 - \frac{I^{\text{plane}}}{I_{d,a}^{\text{plane}}} \end{aligned} \right\} \quad (2.30)$$

By inserting Eq. (2.30) in the Nernst condition (Eq. 2.5), one obtains (see also Chap. 7 of [3]),

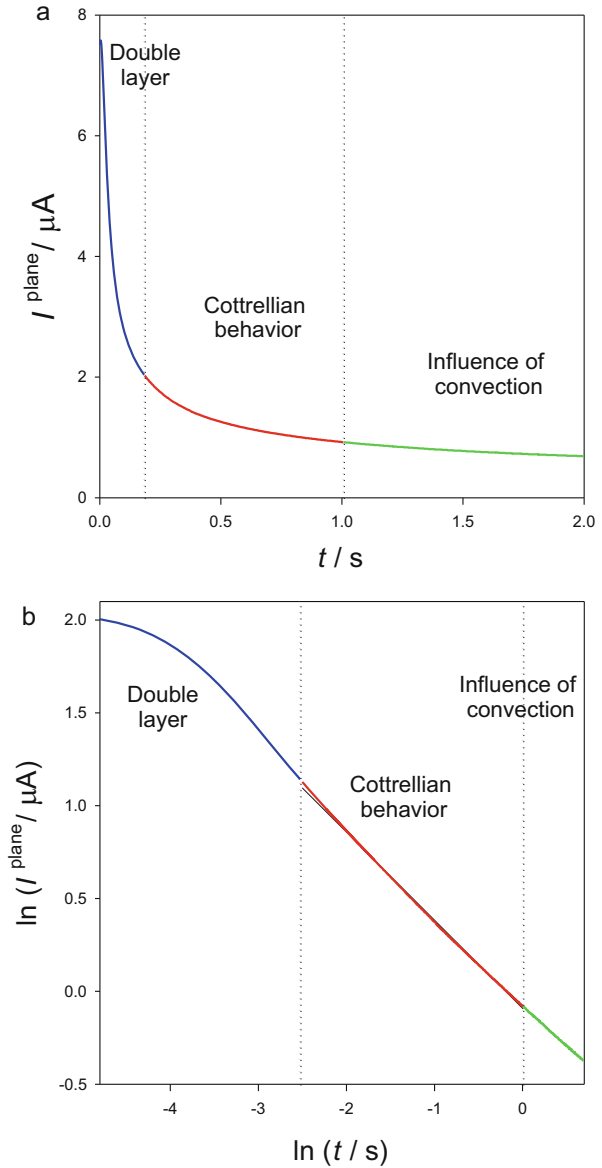
$$E = E_c^{\ominus'} + \frac{RT}{F} \ln \left(\frac{D_{\text{R}}}{D_{\text{O}}} \right)^{1/2} + \frac{RT}{F} \ln \left(\frac{I_{d,c}^{\text{plane}} - I^{\text{plane}}}{I^{\text{plane}} - I_{d,a}^{\text{plane}}} \right) \quad (2.31)$$

$$\text{So, for } I^{\text{plane}} = (I_{d,c}^{\text{plane}} + I_{d,a}^{\text{plane}})/2,$$

³ Natural convection associated to temperature or density gradients or vibrations is present in the usual experiments [14–16].

⁴ Enhancement of the diffusion flux at the edge of an inlaid electrode.

Fig. 2.3 Experimental current–time curve (a) and logarithmic curves (b) for the application of a constant potential to a graphite disc electrode of radius 0.5 mm (planar electrode) for the reduction of $\text{Fe}(\text{CN})_6^{3-}$. $c_{\text{Fe}(\text{CN})_6^{3-}}^* = 2 \text{ mM}$, $A = 0.0078 \text{ cm}^2$, $T = 298 \text{ K}$, $E = -0.1 \text{ V vs. Ag/AgCl, KCl (saturated)}$. From the logarithmic analysis in (b) (restricted to the Cottrellian region, i.e., the red line), the following values have been obtained: slope: -0.48 , intercept: -0.475 . The diffusion coefficient of $\text{Fe}(\text{CN})_6^{3-}$ obtained by applying Eq. (2.29) is $1.15 \times 10^{-6} \text{ cm}^2 \text{ s}^{-1}$



$$E = E_{1/2}^r = E_c^{\ominus'} + \frac{RT}{F} \ln \left(\frac{D_R}{D_O} \right)^{1/2} \quad (2.32)$$

- Another important point of the I – E curve is the crossing potential or “equilibrium potential” for which the current takes a null value, $I^{\text{plane}} = 0$ (see Fig. 2.4a). By inserting this condition in Eq. (2.27),

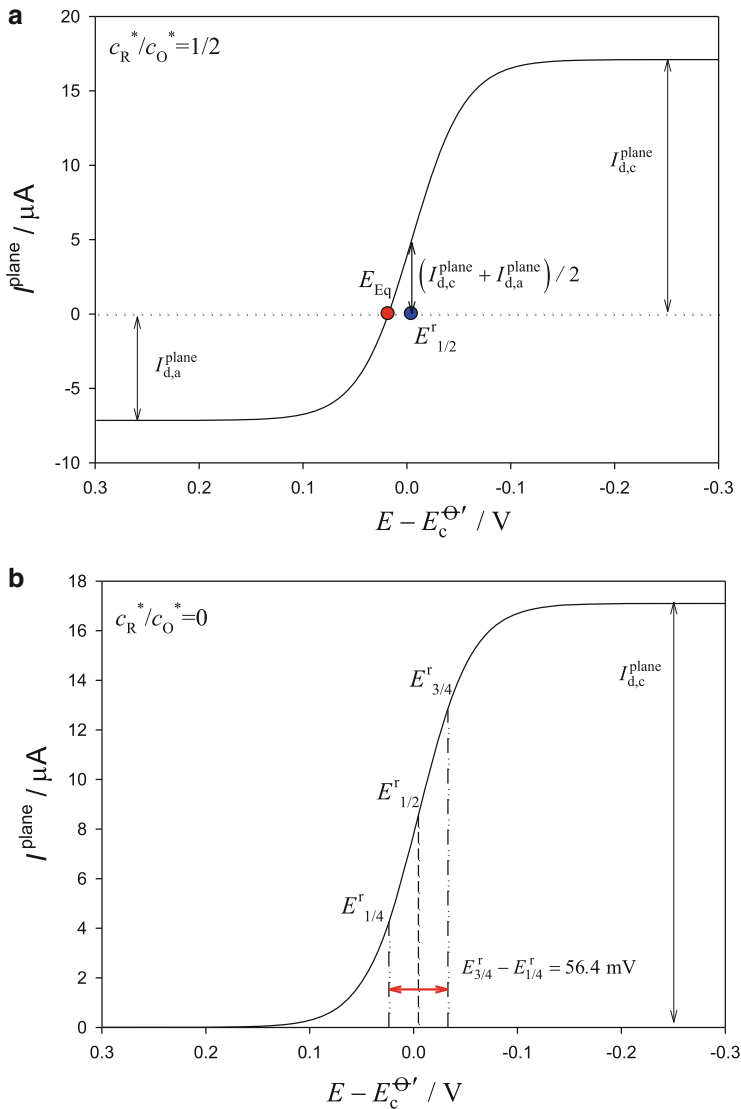


Fig. 2.4 Current–potential curve corresponding to the application of constant potentials to a planar macroelectrode, calculated from Eq. (2.27) with $c_R^*/c_O^* = 0.5$ (a) and 0 (b). $t = 0.1 \text{ s}$, $A = 0.031 \text{ cm}^2$, $D_O = 10^{-5} \text{ cm}^2 \text{ s}^{-1}$, $\gamma = 1.2$

$$E_{\text{Eq}} = E_c^{\Theta'} + \frac{RT}{F} \ln \left(\frac{c_O^*}{c_R^*} \right) \quad (2.33)$$

Otherwise the I – E – t response (Eqs. 2.26 or 2.27), when only the oxidized species O is initially present in the electrolytic solution, is simplified to

$$I^{\text{plane}} = FA \sqrt{\frac{D_O}{\pi t}} \frac{c_O^*}{1 + \gamma e^\eta} = FAD_O \frac{(c_O^* - c_O^{s,r})}{\sqrt{\pi D_O t}} = FAD_R \frac{c_R^{s,r}}{\sqrt{\pi D_R t}} \quad (2.34)$$

Under these conditions only a cathodic wave is obtained (see Fig. 2.4b) and Eq. (2.31) takes the simpler form:

$$E = E_{1/2}^r + \frac{RT}{F} \ln \left(\frac{I_{d,c}^{\text{plane}} - I^{\text{plane}}}{I^{\text{plane}}} \right) \quad (2.35)$$

with the normalized current–potential curve having the following time-independent expression:

$$\frac{I^{\text{plane}}}{I_{d,c}^{\text{plane}}} = \frac{1}{1 + e^{\frac{F}{RT}(E - E_{1/2}^r)}} = \frac{1}{1 + \gamma e^\eta} \quad (2.36)$$

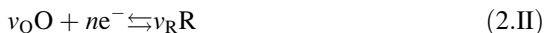
This is a consequence of the form of the reversible I – E – t response.

Note that the plot of E vs. $\ln \left(\left(I_{d,c}^{\text{plane}} - I^{\text{plane}} \right) / \left(I^{\text{plane}} - I_{d,a}^{\text{plane}} \right) \right)$ (or vs. $\ln \left(\left(I_{d,c}^{\text{plane}} - I^{\text{plane}} \right) / I^{\text{plane}} \right)$ when R species is not initially present) is linear with a slope 26 mV (if $T = 298$ K) and intercept equal to $E_{1/2}^r$. This slope is characteristic of reversible charge transfer processes. There are other reversibility criteria based on the difference between potentials $E_{3/4}^r - E_{1/4}^r$, corresponding to the currents $I^{\text{plane}} = (3/4)I_{d,c}^{\text{plane}}$ and $I^{\text{plane}} = (1/4)I_{d,c}^{\text{plane}}$, with this difference being 56.4 mV (See Chap. 5 of [2]; [17] and Fig. 2.4b).

The analysis of the E vs. $\ln \left(\left(I_{d,c}^{\text{plane}} - I^{\text{plane}} \right) / \left(I^{\text{plane}} - I_{d,a}^{\text{plane}} \right) \right)$ curve provides not only a reversibility criteria (from the measurement of the slope of the resulting linear plots), but also provides direct evidence that only one electron has been transferred and a direct measurement of the reversible half-wave potential, $E_{1/2}^r$, which is a fundamental parameter of the redox system in a given supporting electrolyte solution. $E_{1/2}^r$ is closely related to the formal potential (Eq. 2.32) and affected by the diffusion coefficients of the oxidized and reduced species. The half-wave potential varies with the size and shape of the electrode used because it depends on the characteristics of mass transport considered (see Fig. 2.21 in Sect. 2.6).

2.2.3 Stoichiometric Coefficients Different From the Unity

A variation of reaction Scheme (2.1) is considered here by assuming other stoichiometries, in line with the reaction scheme [1, 2]:



where n is the number of electrons transferred and ν_O and ν_R the stoichiometric coefficients of species O and R, respectively.

The mass transport and the initial conditions are also given by Eqs. (2.2) and (2.3), but the surface conditions are now

$t > 0, x = 0$:

$$\frac{D_O}{\nu_O} \left(\frac{\partial c_O}{\partial x} \right)_{x=0} = - \frac{D_R}{\nu_R} \left(\frac{\partial c_R}{\partial x} \right)_{x=0} \quad (2.37)$$

$$(c_O^{s,r})^{\nu_O} = e^\eta (c_R^{s,r})^{\nu_R} \quad (2.38)$$

where η is given by Eq. (2.6).

As previous sections, by using the variable s_i^p (Eq. 2.8), the differential equation system (2.2) and the surface conditions (2.37) and (2.38) become dependent only on s_i^p variable:

$$\frac{\sqrt{D_O}}{\nu_O} \left(\frac{\partial c_O}{\partial s_O^p} \right)_{s_O^p=0} = - \frac{\sqrt{D_R}}{\nu_R} \left(\frac{\partial c_R}{\partial s_R^p} \right)_{s_R^p=0} \quad (2.39)$$

$$(c_O(s_O^p = 0))^{\nu_O} = e^\eta (c_R(s_R^p = 0))^{\nu_R} \quad (2.40)$$

Therefore, the surface fluxes and concentration profiles of species i ($i = O, R$) are also expressed by Eqs. (2.16)–(2.18). From Eqs. (2.17), (2.39), and (2.40), it is possible to obtain the expression for the relationship between the potential and the surface concentration of species O:

$$E = E_c^{\ominus'} + \frac{RT}{nF} \ln \left(\frac{(c_O^{s,r})^{\nu_O}}{\left(\frac{\nu_R}{\nu_O} \gamma \right)^{\nu_R} (c_O^* - c_O^{s,r})^{\nu_R}} \right) \quad (2.41)$$

with γ given by Eq. (2.21).

The expression of the current is

$$I^{\text{plane}} = \frac{FAD_O}{\sqrt{\pi D_O t}} \frac{(c_O^* - c_O^{s,r})}{\nu_O} \quad (2.42)$$

with the limiting current being

$$I_{d,c}^{\text{plane}} = \frac{FAD_O}{\sqrt{\pi D_O t}} \frac{c_O^*}{\nu_O} \quad (2.43)$$

By solving $c_O^{s,r}$ and c_O^* in Eqs. (2.42) and (2.43) and inserting them into (2.41), it is obtained

$$E = E_c^{\Theta'} + \frac{RT}{nF} \ln \left(\frac{v_O v_O}{(v_R \gamma)^{v_R}} \left(\frac{\sqrt{\pi t}}{FA \sqrt{D_O}} \right)^{v_O - v_R} \frac{(I_{d,c}^{\text{plane}} - I^{\text{plane}})^{v_O}}{(I_{d,c}^{\text{plane}})^{v_R}} \right) \quad (2.44)$$

Equation (2.44) transforms into (2.31) for the case $v_O = v_R = 1$ (with $I_{d,a} = 0$). The expression of the half-wave potential is obtained by making $I^{\text{plane}} = I_{d,c}^{\text{plane}}/2$ in (2.44),

$$E_{1/2}^r = E_c^{\Theta'} + v_R \frac{RT}{nF} \ln \left(\frac{D_R}{D_O} \right)^{1/2} + \frac{RT}{nF} \ln \left(\frac{(C_O^*)^{v_O - v_R}}{2^{v_O - v_R} \left(\frac{v_R}{v_O} \right)^{v_R}} \right) \quad (2.45)$$

From these expressions of the half-wave potential it can be inferred that, under these conditions, it depends on the bulk concentration of oxidized species and on the particular values of v_O and v_R .

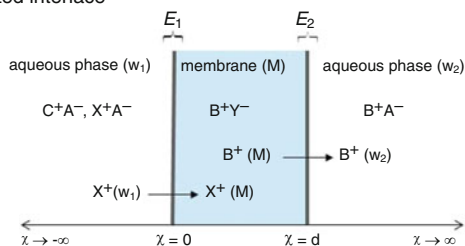
2.3 Ion Transfer Through Liquid Membranes

The study of the ion transfer through artificial liquid membrane systems is important for the elucidation of the ion transfer through biological membranes. In this respect, the Interface between two immiscible electrolyte solutions (ITIES) constitutes a biomimetic medium suitable for studying several fundamental processes, ranging from biocatalysis to cellular respiration of photosynthesis, and many others [18–22]. The first studies of liquid/liquid interfaces (L/L) under the application of an external potential were carried out by Gavach et al. [23], laying the basis for the current electrochemical treatments of ITIES.

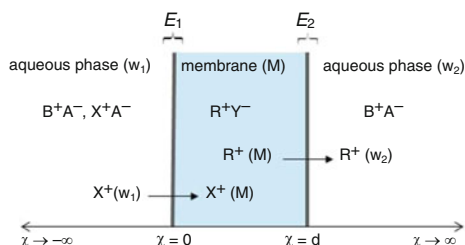
The membrane system considered here is composed of two aqueous solutions w_1 and w_2 , separated by a liquid membrane M, and it involves two aqueous solution/membrane interfaces: w_1/M (outer interface) and M/w_2 (inner interface). If the different ohmic drops (and the potentials caused by mass transfers within w_1 , M, and w_2) can be neglected, the membrane potential, E_M , defined as the potential difference between w_1 and w_2 , is caused by ion transfers taking place at both L/L interfaces. The current associated with the ion transfer across the L/L interfaces is governed by the same mass transport limitations as redox processes on a metal electrode/solution interface. Provided that the ion transport is fast, it can be considered that it is governed by the same diffusion equations, and the electrochemical methodology can be transposed en bloc [18, 24]. With respect to the experimental cell used for electrochemical studies with these systems, it is necessary to consider three sources of resistance, i.e., both the two aqueous and the nonaqueous solutions, with both ITIES sandwiched between them. Therefore, a potentiostat with two reference electrodes is usually used.

Scheme 2.2 A schematic view of the systems with one (a) and two (b) polarized liquid/liquid interfaces: outer (w_1/M) and inner (M/w_2)

a One polarized interface



b Two polarized interfaces



The ion transport through membrane systems can be studied in two forms:

- By using a common ion in the organic membrane and in one of the aqueous phases, such that it can be assumed that the external polarization is only effective at one interface of the membrane, and the current corresponding to a given applied potential is only determined by the transfer of the target ion at one of the interfaces, since the other acts as a reference interface (see Scheme 2.2a).
- In the case of a very hydrophobic supporting electrolyte in the membrane for which it is not possible to have a common ion in the electrolyte of the aqueous phases, a design like that shown in Scheme 2.2b is used. In this situation, both liquid/liquid interfaces in the membrane system are polarized (and the charge transfer reactions are linked to each other through the fulfillment of the electroneutrality of the membrane). These polarization phenomena can be described in terms of the individual electrochemical processes occurring at the two interfaces, which are coupled by virtue of the same intensity of electrical current (in order to maintain the electroneutrality of this system). Moreover, Kihara et al. demonstrated that the useful potential window that this system provides is much wider than that available when only one interface w_1/M is polarized [25–27].

2.3.1 One-Polarized Interface Systems

Many of the systems used for electrochemical studies of ion transfer processes taking place at the ITIES are systems of a single polarized interface. In these kinds of systems, the polarization phenomenon is only effective at the sample solution/

membrane interface, since the potential drop through the other interface is kept constant whatever the nature of this interface (i.e., either liquid/liquid or solid/liquid [28]). In the specific case of a membrane system that separates two aqueous solutions, the non-polarizable interface is achieved by adding a sufficiently high concentration of a common ion in the membrane and inner aqueous solution, by choosing as supporting electrolyte two salts of this common ion with lipophilic and hydrophilic counterions, respectively.

Let us consider the transfer of a cation X^+ between the aqueous phase (w_1) and the organic phase (M),



The distribution of the cation X^+ between both phases in contact leads to the development of a potential drop across the interface,

$$\Delta_M^{w_1} \phi = \phi(w_1) - \phi(M) \quad (2.46)$$

where $\phi(p)$ is the inner potential of the phase p ($= w_1$ or M). This equilibrium potential difference, when X^+ is the only ion that can be transferred, obeys the Nernst equation:

$$\Delta_M^{w_1} \phi = \Delta_M^{w_1} \phi_{X^+}^{\ominus} + \frac{RT}{F} \ln \left(\frac{a_{X^+}^M}{a_{X^+}^{w_1}} \right) = \Delta_M^{w_1} \phi_{X^+}^{\ominus'} + \frac{RT}{F} \ln \left(\frac{c_{X^+}^M}{c_{X^+}^{w_1}} \right) \quad (2.47)$$

with $\Delta_M^{w_1} \phi_{X^+}^{\ominus'}$ being the formal ion transfer potential given by

$$\Delta_M^{w_1} \phi_{X^+}^{\ominus'} = \Delta_M^{w_1} \phi_{X^+}^{\ominus} + \frac{RT}{F} \ln \left(\frac{f_{X^+}^M}{f_{X^+}^{w_1}} \right) \quad (2.48)$$

where R , T , and F have their usual meaning and $a_{X^+}^p$, $f_{X^+}^p$, and $c_{X^+}^p$ are the activity, activity coefficient, and concentration, respectively, of the ion X^+ in the phase p ($= w_1$ or M). $\Delta_M^{w_1} \phi_{X^+}^{\ominus}$ is the standard ion transfer potential, which is related to the standard Gibbs energy of the transfer of X^+ ,

$$\Delta_M^{w_1} \phi_{X^+}^{\ominus} = \frac{\Delta_{w_1}^M G_{X^+}^{\ominus}}{F} \quad (2.49)$$

The standard Gibbs energy of the ion transfer is a direct measurement of lipophilicity, and is related to the standard partition coefficient of the ion in the biphasic system through the following equation:

$$P_{X^+} = \exp \left(- \frac{\Delta_{w_1}^M G_{X^+}^{\ominus}}{RT} \right) \quad (2.50)$$

From the transposition of the theory for NPV to the study of the uptake of a target ion X^+ from an aqueous sample solution to a liquid membrane, the theoretical

equations obtained with the semi-infinite diffusion model can be used to quantify the current response of the ion transfer. The major difference between ionic transfer through and membrane and electronic transfer at a solid electrode is that the boundary condition corresponding to the flux conservation is given by

$$D_{X^+}^{w_1} \left(\frac{\partial c_{X^+}^{w_1}}{\partial x} \right)_{x=0} = D_{X^+}^M \left(\frac{\partial c_{X^+}^M}{\partial x} \right)_{x=0} \quad (2.51)$$

since the concentration of ion X^+ decreases from the aqueous bulk to the membrane surface (i.e., for $-\infty \leq x \leq 0$) and decreases from the membrane surface to the membrane bulk (i.e., for $0 \leq x \leq \infty$). However, as the planar diffusion operator is symmetrical with respect to the x -coordinate, this change does not affect the solution of the differential diffusion equations. So, the equation for the current in NPV of a reversible ion transfer can be written as

$$\left. \begin{aligned} \frac{I}{I_d} &= \frac{\gamma e^\eta}{1 + \gamma e^\eta} \\ E &= E_{1/2}^r + \frac{RT}{F} \ln \left(\frac{I}{I_d - I} \right) \end{aligned} \right\} \quad (2.52)$$

where

$$E_{1/2}^r = \Delta_M^{w_1} \phi_{X^+}^{\ominus'} + \frac{RT}{F} \ln \left(\frac{1}{\gamma} \right) \quad (2.53)$$

$$I_d = FA c_{X^+}^* \sqrt{\frac{D_{X^+}^{w_1}}{\pi t}} \quad (2.54)$$

$$\eta = \frac{F}{RT} \left(E - \Delta_M^{w_1} \phi_{X^+}^{\ominus'} \right) \quad (2.55)$$

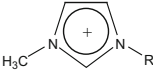
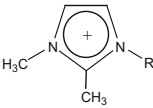
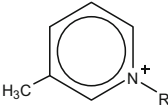
$$\gamma = \left(\frac{D_{X^+}^M}{D_{X^+}^{w_1}} \right)^{1/2} \quad (2.56)$$

with $\Delta_M^{w_1} \phi_{X^+}^{\ominus'}$ being given by Eq. (2.48). From Eq. (2.52), $E_{1/2}^r$ can be easily determined and also the standard ion transfer potential $\Delta_M^{w_1} \phi_{X^+}^{\ominus}$ once the diffusion coefficients are known. Table 2.1 shows the values of $\Delta_M^{w_1} \phi_{X^+}^{\ominus}$ for some ionic liquid cations.

2.3.2 Two-Polarized Interfaces Systems

In these kinds of systems, the polarization phenomenon is effective at the two interfaces involved. Specifically, in membrane systems comprising two ITIES, this

Table 2.1 Standard ion transfer potentials of different *N,N*-alkylimidazolium and 1-butyl-4-methylpyridinium ionic liquid cations [29]

Cation type	R	$\Delta_M^w \phi_{X^+}^-$ (mV)	$\Delta_{w_1}^M G_{X^+}^-$ (kJ/mol)
	C ₄ H ₉	−24.2	−2.33
	C ₆ H ₅	−53.2	−5.13
	C ₆ H ₁₃	−93.2	−8.99
	C ₈ H ₁₇	−162.5	−15.68
	C ₄ H ₉	−35.2	−3.39
	C ₄ H ₉	−51.5	−4.97

behavior is achieved when the membrane contains a hydrophobic supporting electrolyte and the sample aqueous solution (the inner one) contains hydrophilic supporting electrolytes, and there is no common ion between any of the adjacent phases. In this case, the potential drop cannot be controlled individually and the processes taking place at both interfaces are linked to each other by virtue of the same electrical current intensity. Systems of two-polarized interfaces have shown a series of peculiarities that can be advantageous when studying ion transfer processes. Indeed, they provide a potential window about twice that of one-polarized interface systems, the signals of cations and anions with similar standard ion transfer potential values appear widely separated when these systems are used, and the half-wave potential of the ions in these systems is influenced by their concentration.

In Scheme 2.2b interface w_1/M is the outer or working interface, and interface M/w_2 is the inner interface (not a reference interface).

The theoretical characterization of the response of this kind of membrane systems in electrochemical techniques is very interesting for determining thermodynamics and transport parameters of ions.

According to Scheme 2.2b, to solve this problem we must find the following unknown variables.

- At interface w_1/M : The concentration profiles of the target cation at both sides of this interface ($c_{X^+}^{w_1}$ and $c_{X^+}^M$) and the potential drop E_1 .
- At interface M/w_2 : The concentration profiles of the cation R^+ of the supporting electrolyte of the membrane at both sides of this interface ($c_{R^+}^M$ and $c_{R^+}^{w_2}$) and the potential drop E_2 . Note that it has been assumed that R^+ is being transferred at the inner interface, coupled with the transfer of X^+ at the outer one, in order to maintain electroneutrality.

$c_{X^+}^*$ and $c_{R^+}^*$ are the initial concentrations of the target ion in aqueous phase w_1 and of the electrolyte cation R^+ in the membrane, respectively.

Indeed, this is a problem with five unknown variables, the four concentrations above indicated and one of the potential differences at the two interfaces, E_1 or E_2 , since they can be reduced to one potential difference because $E_M = E_1 - E_2$ is known. Four differential equations and the additional condition of equality of the fluxes of the target ion X^+ and the cation R^+ at the outer and inner interfaces, respectively, will be used to obtain the explicit I/E_M curve and the concentration profiles of all the species.

Interface w_1/M or Outer Interface

The differential equations and the boundary value problem (bvp) which can be fulfilled by $c_{X^+}^{w_1}$ and $c_{X^+}^M$ if the thickness of the membrane is greater than the diffusion layer of X^+ into the membrane are:

$$\frac{\partial c_{X^+}^{w_1}}{\partial t} = D_{X^+}^{w_1} \frac{\partial^2 c_{X^+}^{w_1}}{\partial x^2} \quad (2.57)$$

$$\frac{\partial c_{X^+}^M}{\partial t} = D_{X^+}^M \frac{\partial^2 c_{X^+}^M}{\partial x^2} \quad (2.58)$$

in phase w_1 :

$$\left. \begin{array}{l} t = 0, \quad x < 0 \\ t \geq 0, \quad x \rightarrow -\infty \end{array} \right\} c_{X^+}^{w_1} = c_{X^+}^* \quad (2.59)$$

in phase M:

$$\left. \begin{array}{l} t = 0, \quad 0 < x < d \\ t \geq 0, \quad x \rightarrow d \end{array} \right\} c_{X^+}^M = 0 \quad (2.60)$$

$t > 0, \quad x = 0$:

$$c_{X^+}^M = e^{\eta_1} c_{X^+}^{w_1} \quad (2.61)$$

$$D_{X^+}^{w_1} \left(\frac{\partial c_{X^+}^{w_1}}{\partial x} \right)_{x=0} = D_{X^+}^M \left(\frac{\partial c_{X^+}^M}{\partial x} \right)_{x=0} \quad (2.62)$$

with

$$\eta_1 = \frac{F}{RT} (E_1 - \Delta_M^{w_1} \phi_{X^+}^{\ominus'}) \quad (2.63)$$

and E_1 is unknown.

Interface M/w₂ or Inner Interface

$$\frac{\partial c_{R^+}^{w_2}}{\partial t} = D_{R^+}^{w_2} \frac{\partial^2 c_{R^+}^{w_2}}{\partial x^2} \quad (2.64)$$

$$\frac{\partial c_{R^+}^M}{\partial t} = D_{R^+}^M \frac{\partial^2 c_{R^+}^M}{\partial x^2} + \text{migration term} \quad (2.65)$$

Inside the membrane, the transport of R^+ takes place by diffusion and ionic migration and is described by a very complex differential equation. However, since the current is controlled by the diffusion of the target ion X^+ and since $c_{R^+}^*$ in membrane is high enough, it will be assumed that the R^+ concentration is constant in all the membranes, i.e., in $0 < x < d$. Therefore, Eq. (2.65) can be changed for the following condition:

$$c_{R^+}^M(x, t) = c_{R^+}^* \quad (2.66)$$

in phase M:

$$\left. \begin{array}{l} t = 0, \quad 0 < x < d \\ t \geq 0, \quad x \rightarrow d \end{array} \right\} c_{R^+}^M = c_{R^+}^* \quad (2.67)$$

in phase w₂:

$$\left. \begin{array}{l} t = 0, \quad x \geq d \\ t \geq 0, \quad x \rightarrow \infty \end{array} \right\} c_{R^+}^{w_2} = 0 \quad (2.68)$$

$$t > 0, \quad x = d : c_{R^+}^M = e^{\eta_2} c_{R^+}^{w_2} \quad (2.69)$$

or, according with (2.66):

$$c_{R^+}^* = e^{\eta_2} c_{R^+}^{w_2} \quad (2.70)$$

where

$$\eta_2 = \frac{F}{RT} (E_2 - \Delta_{w_2}^M \phi_{R^+}^{\ominus'}) \quad (2.71)$$

and E_2 is unknown.

The solutions of both problems are simple due to their separate character, with each of them corresponding to the response of reversible charge transfer processes, in such a way that the following is obtained for interface w₁/M:

$$I_1 = FA \sqrt{\frac{D_{X^+}^{w_1}}{\pi t}} (c_{X^+}^* - c_{X^+}^{w_1}(0)) \quad (2.72)$$

and

$$E_1 = \Delta_M^{w_1} \phi_{X^+}^{\ominus'} + \frac{RT}{F} \ln \left(\frac{1}{\gamma_1} \right) + \frac{RT}{F} \ln \left(\frac{I_1}{I_d - I_1} \right) \quad (2.73)$$

with

$$I_d = FA \sqrt{\frac{D_{X^+}^{w_1}}{\pi t}} c_{X^+}^* \quad (2.74)$$

$$\gamma_1 = \sqrt{\frac{D_{X^+}^M}{D_{X^+}^{w_1}}} \quad (2.75)$$

For the interface M/w₂:

$$I_2 = FA \sqrt{\frac{D_{R^+}^{w_2}}{\pi t}} c_{R^+}^{w_2}(d) \quad (2.76)$$

By taking into account that the transfer of R⁺ through M/w₂ interface also occurs reversibly, and that the current through both interfaces is the same, i.e., $I_1 = I_2 = I$, it can be deduced:

$$E_2 = \Delta_{w_2}^M \phi_{X^+}^{\ominus'} + \frac{RT}{F} \ln \left(\frac{c_{R^+}^*}{\gamma_2 c_{X^+}^*} \right) + \frac{RT}{F} \ln \left(\frac{I_d}{I} \right) \quad (2.77)$$

with

$$\gamma_2 = \sqrt{\frac{D_{X^+}^{w_1}}{D_{R^+}^{w_2}}} \quad (2.78)$$

By subtracting equations for E_1 and E_2 ,

$$E^M = E_2 - E_1 = E_{1/2}^M + \frac{RT}{F} \ln \left(\frac{2(I_N)^2}{1 - I_N} \right) \quad (2.79)$$

where:

$$I_N = \frac{I(t)}{I_d(t)} \quad (2.80)$$

$$E_{1/2}^M = E^{M, \ominus'} + \frac{RT}{F} \ln \left(\frac{1}{\lambda} \right) \quad (2.81)$$

$$\lambda = \frac{2\sqrt{D_{R^+}^{w_2} D_{X^+}^M}}{D_{X^+}^{w_1}} \frac{c_{R^+}^*}{c_{X^+}^*} \quad (2.82)$$

$$E^{M, \ominus'} = \Delta_M^{w_1} \phi_{X^+}^{\ominus'} - \Delta_{w_2}^M \phi_{R^+}^{\ominus'} \quad (2.83)$$

Equation (2.79) provides the expression of the membrane potential E^M (applied potential) as a function of the normalized current I_N at this potential (measured current, which is not known). So, by working out the current from the above equation we deduce the following explicit expression for the current obtained in single potential step voltammetry as a function of the applied potential:

$$I = FA \sqrt{\frac{D_{X^+}^w}{\pi t}} c_{X^+}^* g(\eta) \quad (2.84)$$

where $g(\eta)$ is the function that contains the dependence on the applied potential for this kind of membrane systems and it is also fundamental in the current–potential response deduced for any voltammetric technique [30],

$$\left. \begin{aligned} g(\eta) &= \frac{\sqrt{\lambda^2 e^{2\eta} + 8\lambda e^\eta} - \lambda e^\eta}{4} \\ \eta &= \frac{F}{RT} (E^M - E^{M, \ominus'}) \end{aligned} \right\} \quad (2.85)$$

If coupled to the transfer of the target cation, through the outer interface, the anion of the supporting electrolyte of w_2 is transferred through the inner one; Eqs. (2.84) and (2.85) are still valid for changing λ for λ^- ,

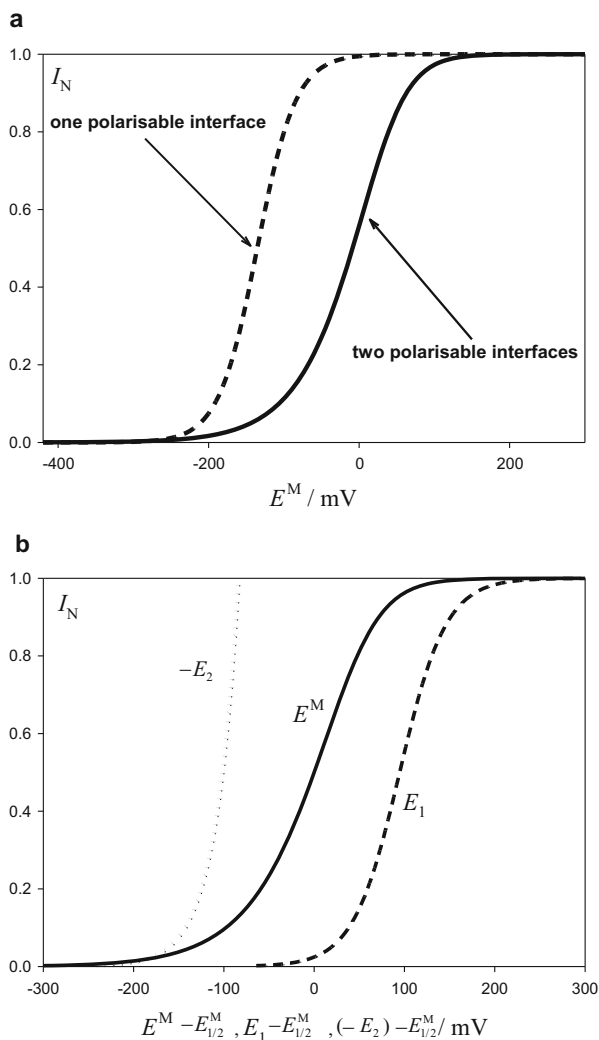
$$\lambda^- = \frac{2\sqrt{D_{R^+}^M D_{X^+}^M}}{D_{X^+}^{w_1}} \frac{c_{R^+}^*}{c_{X^+}^*} \quad (2.86)$$

By comparing this solution with that obtained for only one polarized L/L interface (Eq. 2.52), it can be observed that both are formally similar if we change $g(\eta)$ function for the sigmoidal function $\gamma e^\eta / (1 + \gamma e^\eta)$. The different behavior of both responses is shown in Fig. 2.5, which corresponds to the transfer of a target cation X^+ from water to a plasticized polymeric membrane in a system of one and two L/L polarized interfaces (dashed and solid line, respectively). It can be seen in Figure 2.5a that when the two interfaces are polarized, the I/E curve behaves in a similar way to that corresponding to an irreversible process with only one interface. Figure 2.5b also shows how the I/E curve corresponding to the applied potential (or the membrane potential) is the sum of the curves corresponding to the outer and inner potentials.

Note finally that in the case of two-polarized interface systems, the plots of the membrane potential E^M versus $\ln(2(I_N)^2 / (1 - I_N))$ are linear with a slope equal to RT/F and an intercept $E_{1/2}^M$.

Fig. 2.5 (a) Normalized current–potential curves corresponding to a system with two polarizable liquid/liquid interfaces (*solid line*; see Eq. (2.84)) and to a system with one polarizable interface (*dashed line*; see Eq. (2.52)). (b) I_N/E^M (*solid line*), I_N/E_1 (*dashed line*), and $I_N/(-E_2)$ (*dotted line*) calculated from Eqs. (2.84), (2.73), and (2.77), respectively.

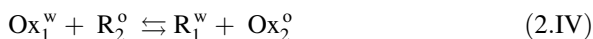
$\Delta_M^{w_1} \phi_{X^+}^{\ominus'} = -224 \text{ mV}$,
 $\Delta_{w_2}^M \phi_{R^+}^{\ominus'} = -304 \text{ mV}$,
 $D_{X^+}^{w_1} = D_{R^+}^{w_2} = 10^{-5} \text{ cm}^2 \text{ s}^{-1}$,
 $D_{X^+}^M = 10^{-8} \text{ cm}^2 \text{ s}^{-1}$,
 $c_{X^+}^* = 0.1 \text{ mM}$,
 $c_{R^+}^* = 50 \text{ mM}$, $T = 298.15 \text{ K}$.
 Reproduced with permission [30]



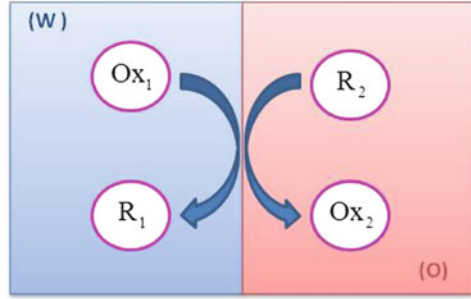
2.3.3 Electron Transfer at the Liquid/Liquid Interface

In this section, we will consider the transfer of electrons between an oxidized species O_1 in an aqueous phase and a reduced species R_1 in an organic phase, as illustrated in reaction Scheme 2.3

The global process can be written as



Scheme 2.3 A schematic view of an heterogeneous redox reaction at a liquid/liquid interface



To solve the mass transport equations corresponding to this process, it is necessary to consider the arrival of two reactants in different phases at the surface and the departure of the two products from it, so four differential equations should be considered [31]: two for the aqueous phase,

$$\left. \begin{aligned} \frac{\partial c_{Ox_1}}{\partial t} &= D_{O_1} \frac{\partial^2 c_{Ox_1}}{\partial x^2} \\ \frac{\partial c_{R_1}}{\partial t} &= D_{R_1} \frac{\partial^2 c_{R_1}}{\partial x^2} \end{aligned} \right\} \quad (2.87)$$

and two for the organic one,

$$\left. \begin{aligned} \frac{\partial c_{Ox_2}}{\partial t} &= D_{O_2} \frac{\partial^2 c_{Ox_2}}{\partial x^2} \\ \frac{\partial c_{R_2}}{\partial t} &= D_{R_2} \frac{\partial^2 c_{R_2}}{\partial x^2} \end{aligned} \right\} \quad (2.88)$$

The boundary value problem is the following:

$$t = 0, \quad \forall x$$

$$\left. \begin{aligned} c_{Ox_1} &= c_{Ox_1}^* \\ c_{R_1} &= c_{R_1}^* \\ c_{Ox_2} &= c_{Ox_2}^* \\ c_{R_2} &= c_{R_2}^* \end{aligned} \right\} \quad (2.89)$$

$$t > 0, \quad x \rightarrow -\infty$$

$$\left. \begin{aligned} c_{Ox_1} &= c_{Ox_1}^* \\ c_{R_1} &= c_{R_1}^* \end{aligned} \right\} \quad (2.90)$$

$t > 0, \quad x \rightarrow \infty$

$$\left. \begin{aligned} c_{O_2} &= c_{O_2}^* \\ c_{R_2} &= c_{R_2}^* \end{aligned} \right\} \quad (2.91)$$

$t > 0, \quad x = 0$

$$\left. \begin{aligned} D_{Ox_1} \left(\frac{\partial c_{Ox_1}}{\partial x} \right)_{x=0} + D_{R_1} \left(\frac{\partial c_{R_1}}{\partial x} \right)_{x=0} &= 0 \\ D_{Ox_2} \left(\frac{\partial c_{Ox_2}}{\partial x} \right)_{x=0} + D_{R_2} \left(\frac{\partial c_{R_2}}{\partial x} \right)_{x=0} &= 0 \end{aligned} \right\} \quad (2.92)$$

The solutions to the four differential equations given by Eqs. (2.87) and (2.88) can be obtained easily by introducing the s_i^p parameter defined in Eq. (2.8). Once this parameter is inserted in the above equations, the following general solution for the concentration profiles is obtained by following a similar procedure to that described in Sect. 2.2:

$$c_i(x, t) = c_i^* + (c_i(0) - c_i^*) \operatorname{erfc}(s_i^p) \quad \text{with } i = Ox_1, R_1, Ox_2, \text{ and } R_2 \quad (2.93)$$

Note that $\operatorname{erfc}(x) = 1 - \operatorname{erf}(x)$ for $x > 0$ and $\operatorname{erfc}(x) = 1 + \operatorname{erf}(x)$ for $x < 0$.

From this equation, it is possible to calculate the surface gradients of the four species. If we assume that the diffusion coefficients of all of them are equal ($D_{Ox_1} = D_{R_1} = D_{Ox_2} = D_{R_2} = D$), then,

$$\left. \begin{aligned} \left(\frac{\partial c_{Ox_1}}{\partial x} \right)_{x=0} &= - \frac{(c_{Ox_1}(0) - c_{Ox_1}^*)}{\sqrt{\pi D t}} \\ \left(\frac{\partial c_{R_1}}{\partial x} \right)_{x=0} &= - \frac{(c_{R_1}(0) - c_{R_1}^*)}{\sqrt{\pi D t}} \\ \left(\frac{\partial c_{Ox_2}}{\partial x} \right)_{x=0} &= \frac{(c_{Ox_2}(0) - c_{Ox_2}^*)}{\sqrt{\pi D t}} \\ \left(\frac{\partial c_{R_2}}{\partial x} \right)_{x=0} &= \frac{(c_{R_2}(0) - c_{R_2}^*)}{\sqrt{\pi D t}} \end{aligned} \right\} \quad (2.94)$$

The current is given by the following relationship:

$$I = FAD \left(\frac{\partial c_{Ox_1}}{\partial x} \right)_{x=0} \quad (2.95)$$

Taking into account Eqs. (2.92), (2.94), and (2.95), we get the following expressions for the surface concentrations of the four species in terms of the current:

$$\left. \begin{aligned} c_{\text{Ox}_1}(0) &= \frac{-I}{FA\sqrt{\frac{D}{\pi t}}} + c_{\text{Ox}_1}^* \\ c_{\text{R}_1}(0) &= \frac{I}{FA\sqrt{\frac{D}{\pi t}}} + c_{\text{R}_1}^* \\ c_{\text{Ox}_2}(0) &= \frac{I}{FA\sqrt{\frac{D}{\pi t}}} + c_{\text{Ox}_2}^* \\ c_{\text{R}_2}(0) &= \frac{-I}{FA\sqrt{\frac{D}{\pi t}}} + c_{\text{R}_2}^* \end{aligned} \right\} \quad (2.96)$$

The equivalent of the Nernst equation for the above process at the interface is

$$\Delta_o^w \phi = \Delta_o^w \phi^{\ominus'} + \frac{RT}{F} \ln \left(\frac{c_{\text{R}_1}(0)c_{\text{Ox}_2}(0)}{c_{\text{Ox}_1}(0)c_{\text{R}_2}(0)} \right) \quad (2.97)$$

which can be rewritten as

$$e^\eta = \frac{c_{\text{R}_1}(0)c_{\text{Ox}_2}(0)}{c_{\text{Ox}_1}(0)c_{\text{R}_2}(0)} = \left(\frac{\left(I_N + \frac{c_{\text{R}_1}^*}{c_{\text{Ox}_1}^*} \right) \left(I_N + \frac{c_{\text{Ox}_2}^*}{c_{\text{Ox}_1}^*} \right)}{(-I_N + 1) \left(-I_N + \frac{c_{\text{R}_2}^*}{c_{\text{Ox}_1}^*} \right)} \right) \quad (2.98)$$

with

$$\eta = \frac{F}{RT} \left(\Delta_o^w \phi - \Delta_o^w \phi^{\ominus'} \right) \quad (2.99)$$

$$I_N = \frac{I}{FAc_{\text{Ox}_1}^* \sqrt{\frac{D}{\pi t}}} \quad (2.100)$$

By working out the current in terms of the potential, the following quadratic equation is obtained:

$$I_N^2 (e^\eta - 1) - I_N [e^\eta (1 + \beta) + \alpha + \gamma] + e^\eta \beta - \alpha \gamma = 0 \quad (2.101)$$

with

$$\left. \begin{aligned} \alpha &= \frac{c_{\text{R}_1}^*}{c_{\text{Ox}_1}^*} \\ \beta &= \frac{c_{\text{R}_2}^*}{c_{\text{Ox}_1}^*} \\ \gamma &= \frac{c_{\text{O}_2}^*}{c_{\text{Ox}_1}^*} \end{aligned} \right\} \quad (2.102)$$

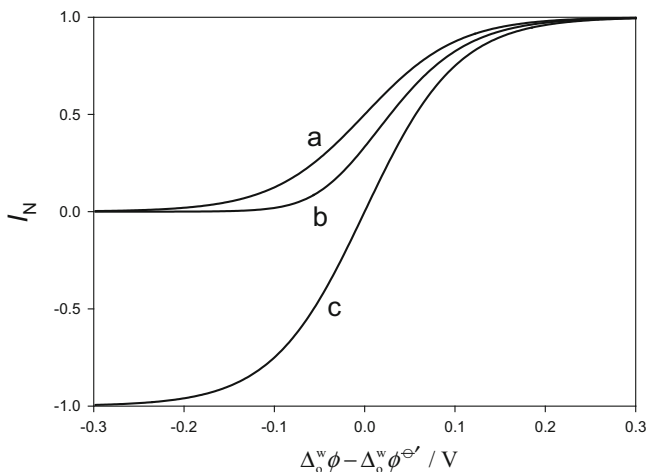


Fig. 2.6 Normalized current–potential curves corresponding to a heterogeneous redox reaction at a liquid/liquid interface calculated from Eqs. (2.102) and (2.103). The values of coefficients α , β , and γ are: (a) 0, 1, and 0; (b) 1, 1, and 0; (c) 1, 1, and 1

Finally, the current corresponds to the following root of Eq. (2.101):

$$I_N = \frac{[e^\eta(1 + \beta) + \alpha + \gamma] - \sqrt{[e^\eta(1 + \beta) + \alpha + \gamma]^2 - 4(e^\eta - 1)(e^\eta\beta - \alpha\gamma)}}{2(e^\eta - 1)} \quad (2.103)$$

Figure 2.6 plots the NPV response of a redox reaction at a liquid/liquid interface for different values of the ratio of concentrations α , β , and γ (see Eq. 2.102). As can be seen in these curves, the presence of the products of the redox reaction at the aqueous phase R_1 leads to a shift of the response toward more positive potentials (curve b), whereas the presence of species O_2 allows the attainment of negative currents for negative values of $\Delta_o^w \phi - \Delta_o^w \phi^{\ominus'}$.

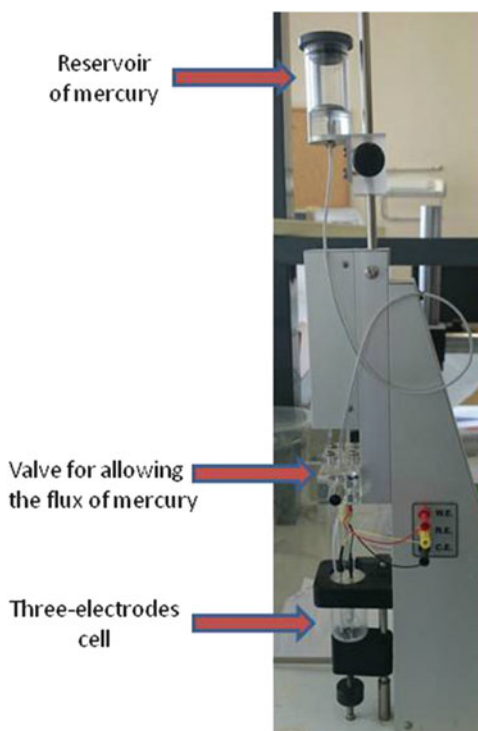
2.4 Dropping Mercury Electrode (DME)

Although nowadays the DME electrode is scarcely employed, it is of a great historical importance since it allowed the development of the first voltammetrical technique, Polarography, designed by Jaroslav Heyrovský (Fig. 2.7). A DME consists of a glass capillary of 0.05–0.1 mm of internal diameter from which mercury flows forming spherical drops (see Fig. 2.8). This electrode has two characteristic parameters: the flow rate m (mass of mercury per unit of time) and the drop life time t_1 . By assuming that the electrode has spherical shape at any

Fig. 2.7 A portrait of Jaroslav Heyrovský, Nobel Prize for Chemistry in 1959 “for his discovery and development of the polarographic methods of analysis.” Source: archiv ÚFCH J. Heyrovského AV ČR, v.v.i. <http://www.jh-inst.cas.cz>



Fig. 2.8 A schematic view of a Dropping Mercury Electrode



moment, the radius and the area of the drop at any instant during its growth are (see Chap. 2 of [3]):

$$r_{\text{DME}} = \left(\frac{3mt}{4\pi\rho} \right)^{1/3} \quad (2.104)$$

$$A(t) = 4\pi r_{\text{DME}}^2 = 4\pi \left(\frac{3mt}{4\pi \times 13.6} \right)^{2/3} = 0.85m^{2/3}t^{2/3} \quad (2.105)$$

with $0 \leq t \leq t_1$, ρ being the mercury density in g cm^{-3} , m being expressed in g s^{-1} , t in s, and the area in cm^2 .

The DME presents special features derived from its homogeneous and isotropic drops, small size, and periodical renewed surface so that the current on each drop rises from zero to its maximum value toward the end of the drop life. Moreover, it is well known that mercury has the highest overpotential for hydrogen evolution, which enables polarization of the electrode to very negative potentials.

Two different ways of operating with a DME will be described in this section. In the first, called “dc Polarography” (dcP), the potential step is applied from the beginning of the drop life with electrolysis taking place during the whole drop life. The other way consists of applying a potential pulse only at the end of the drop life for a short time called pulse time (1–200 ms), after which the potential returns to the initial value. This last technique is called Normal Pulse Polarography (NPP). In the first technique, the voltage varies linearly with time very slowly from an initial value, so it can be considered almost constant for each drop during the whole drop life. The polarographic potential–current curve presents regular oscillations due to the repetitive drop growth and fall. This feature prompted the application of dumping systems, and thus most of the theoretical expressions have been derived for mean currents. As will be seen below, for reversible electrode processes, the instantaneous current during a single drop varies with $t^{1/6}$ following an “Ilkovičian” behavior.

2.4.1 *dc Polarography*

Theoretically, the modeling of the electrochemical response corresponding to the application of a constant potential to a single drop presents an additional complication over stationary electrodes due to the convection caused by the growth of the mercury drop toward the solution. Under these conditions the temporal variation of the concentration of electroactive species is related both to the diffusion component and to convection. This problem was solved by Koutecký by using the expanding sphere electrode model (see Eq. 2.119), although the first model that treated this electrode was proposed by Ilkovič [32], and is known as the “expanding plane” model, and assumes linear diffusion in the way,

$$\frac{\partial c_i}{\partial t} = D_i \frac{\partial^2 c_i}{\partial x^2} - v_x \frac{\partial c_i}{\partial x} \quad i = O, R \quad (2.106)$$

with the term $v_x \partial c_i / \partial x$ being related to the convection through the velocity of the solution, v_x (see Sect. 1.8.3). The basic assumption of the model is that the growth of the drop can be described as the movement of an expanding plane toward the solution, so the convection velocity would be only observed in the normal direction to the plane, v_x . Its expression is $v_x = -2x/3t$, such that the mass transport equation becomes [3, 32–34]:

$$\frac{\partial c_i}{\partial t} = D_i \frac{\partial^2 c_i}{\partial x^2} + \frac{2x}{3t} \frac{\partial c_i}{\partial x} \quad i = O, R \quad (2.107)$$

The applicability of this model is restricted to longer times, i.e., drops of large radius ($r_{\text{DME}} \geq 0.05$ cm for $t = 1$ s). Although this equation is logically more complex than that corresponding to stationary planar electrodes, it can be easily solved in a similar way to that described in Sect. 2.2 (Eqs. 2.8–2.19) by making the following variable change:

$$s_i^{\text{DME}} = \sqrt{\frac{7}{3}} \frac{x}{2\sqrt{D_i t}} = \sqrt{\frac{7}{3}} s_i^{\text{p}} \quad i = O, R \quad (2.108)$$

By including this new variable in the differential equation system (2.107) and in the initial and limiting conditions, these are transformed into a one-variable problem (s_i^{DME}) of identical form to that given by Eqs. (2.9)–(2.12) for static planar electrodes; that is, c_O and c_R can be expressed as functions of only one variable, s_O^{DME} and s_R^{DME} , respectively. Thus, by following the same procedure indicated by Eqs. (2.13)–(2.18), one obtains expressions for the concentration profiles:

$$\left. \begin{aligned} c_O(x, t) &= c_O(s_O^{\text{DME}}) = c_O^* + (c_O^{s,r} - c_O^*) \operatorname{erfc}(s_O^{\text{DME}}) \\ c_R(x, t) &= c_R(s_R^{\text{DME}}) = c_R^* + (c_R^{s,r} - c_R^*) \operatorname{erfc}(s_R^{\text{DME}}) \end{aligned} \right\} \quad (2.109)$$

As can be seen, these expressions are formally identical to those deduced for a planar electrode (compare Eqs. (2.109) and (2.19)), with the only difference being the definition of the dimensionless variable: s_i^{p} for planar electrodes and s_i^{DME} for DME. Under these conditions, surface concentrations are also given by Eq. (2.20) and condition (2.22) is also fulfilled.

According to Fick's law the current is

$$I_{\text{dcP}}^{\text{DME}} = FA(t)D_O \left(\frac{\partial c_O}{\partial x} \right)_{x=0} = -FA(t)D_R \left(\frac{\partial c_R}{\partial x} \right)_{x=0} \quad (2.110)$$

with $A(t)$ given by Eq. (2.105). Inserting Eq. (2.109) in Eq. (2.110), gives the following expression for the current:

$$I_{\text{dcP}}^{\text{DME}} = FA(t)D_{\text{O}}\sqrt{\frac{7}{3\pi D_{\text{O}}t}}(c_{\text{O}}^* - c_{\text{O}}^{\text{s,r}}) = -FA(t)D_{\text{R}}\sqrt{\frac{7}{3\pi D_{\text{R}}t}}(c_{\text{R}}^* - c_{\text{R}}^{\text{s,r}}) \quad (2.111)$$

with $c_{\text{O}}^{\text{s,r}}$ and $c_{\text{R}}^{\text{s,r}}$ being the surface concentrations deduced for a plane electrode given by Eq. (2.20).

From Eq. (2.105), (2.111) can be written as

$$\begin{aligned} I_{\text{dcP}}^{\text{DME}} &= 4\pi\left(\frac{3m}{4\pi\rho}\right)^{2/3}FD_{\text{O}}t^{2/3}\sqrt{\frac{7}{3\pi D_{\text{O}}t}}(c_{\text{O}}^* - c_{\text{O}}^{\text{s,r}}) = \\ &= -4\pi\left(\frac{3m}{4\pi\rho}\right)^{2/3}FD_{\text{R}}t^{2/3}\sqrt{\frac{7}{3\pi D_{\text{R}}t}}(c_{\text{R}}^* - c_{\text{R}}^{\text{s,r}}) \end{aligned} \quad (2.112)$$

and on inserting Eq. (2.20) in (2.112),

$$I_{\text{dcP}}^{\text{DME}} = 4\pi\left(\frac{3m}{4\pi\rho}\right)^{2/3}FD_{\text{O}}t^{1/6}\sqrt{\frac{7}{3\pi D_{\text{O}}}}\frac{(c_{\text{O}}^* - c_{\text{R}}^*e^{\eta})}{1 + \gamma e^{\eta}} \quad (2.113)$$

If we consider that the current I is in A, the concentrations c_i^* are in mol cm^{-3} , the diffusion coefficient D_{O} is in $\text{cm}^2 \text{s}^{-1}$, the mercury density ρ in g cm^{-3} , the mercury flow m in g s^{-1} , and time t in s, Eq. (2.113) becomes

$$I_{\text{dcP}}^{\text{DME}} = 0.732FD_{\text{O}}^{1/2}m^{2/3}\frac{(c_{\text{O}}^* - c_{\text{R}}^*e^{\eta})}{1 + \gamma e^{\eta}}t^{1/6} \quad (2.114)$$

From this equation, cathodic and anodic limits are deduced by making $e^{\eta} \rightarrow 0$ and $e^{\eta} \rightarrow \infty$, respectively, giving rise to the well-known Ilkovič equations [32–34]:

$$\left. \begin{aligned} I_{\text{d,c}}^{\text{DME}} &= 0.732FD_{\text{O}}^{1/2}m^{2/3}c_{\text{O}}^*t^{1/6} \\ I_{\text{d,a}}^{\text{DME}} &= -0.732FD_{\text{R}}^{1/2}m^{2/3}c_{\text{R}}^*t^{1/6} \end{aligned} \right\} \quad (2.115)$$

Figure 2.9 plots the time variation of the limiting current $I_{\text{d,c}}^{\text{DME}}$ given by the Eq. (2.115) for five drops. As can be seen in this Figure, the current increases with time until $t = t_1$ when the drop falls and, logically, the current also falls to zero.

Note that for the DME it is fulfilled that

$$\frac{I_{\text{dcP}}^{\text{DME}}}{I_{\text{d,c}}^{\text{DME}}} = \frac{(1 - (c_{\text{R}}^*/c_{\text{O}}^*)e^{\eta})}{1 + \gamma e^{\eta}} \quad (2.116)$$

which can be rewritten as

$$E = E_{1/2}^{\text{r}} + \frac{RT}{F} \ln \left(\frac{I_{\text{d,c}}^{\text{DME}} - I_{\text{dcP}}^{\text{DME}}}{I_{\text{dcP}}^{\text{DME}} - I_{\text{d,a}}^{\text{DME}}} \right) \quad (2.117)$$

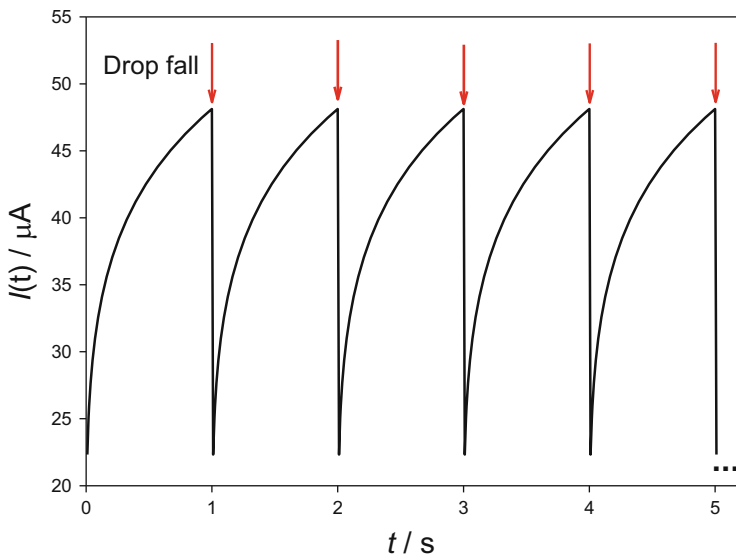


Fig. 2.9 Current–time curves for a DME calculated from Eq. (2.115). $m = 0.1 \text{ g s}^{-1}$, $D_{\text{O}} = 10^{-5} \text{ cm}^2 \text{ s}^{-1}$, $t_1 = 1 \text{ s}$, $c_{\text{O}}^* = 1 \text{ mM}$

Observe that Eqs. (2.116) and (2.117) are identical to (2.27), (2.28) and (2.31) deduced for planar electrodes.

From Eq. (2.111), it can be deduced that the Nernst diffusion layer for a DME is

$$\delta_{\text{DME},i}^r = \sqrt{\frac{3}{7}\pi D_i t} = \sqrt{\frac{3}{7}} \delta_{\text{p},i}^r \quad i = \text{O, R} \quad (2.118)$$

By using the expanding sphere electrode model for the DME, Koutecký obtained the following expression for the instantaneous limiting current [35–37]:

$$I_{\text{dcP}}^{\text{DME}} = 0.732 F D_{\text{O}}^{1/2} m^{2/3} c_{\text{O}}^* t^{1/6} \left\{ 1 + 3.9 \frac{D_{\text{O}}^{1/2} t^{1/6}}{m^{1/3}} + 1.5 \left(\frac{D_{\text{O}}^{1/2} t^{1/6}}{m^{1/3}} \right)^2 + \dots \right\} \quad (2.119)$$

2.4.2 Normal Pulse Polarography (NPP)

In this technique, the DME is kept at an initial potential E_1 during a time t_1 at which the electrode reaction cannot occur and then it is polarized by a potential pulse of increasing amplitude, E_2 . The measurement of the current during a short pulse time t_2 at the end of the drop life confers important advantages on NPP over dcP in relation to the elimination of double-layer effects. In any case, this technique is actually a single potential step technique in which the perturbation shown in

Scheme 2.1 is applied to the DME for a very short time interval, t_2 , before which the electrode has an area proportional to $t_1^{2/3}$.

The differential diffusion equations system to solve when a potential pulse E is applied and the corresponding boundary value problem (bvp) when the expanding plane model for the DME is considered are:

$$\frac{\partial c_i}{\partial t_2} = D_i \frac{\partial^2 c_i}{\partial x^2} + \frac{2x}{3(t_1 + t_2)} \frac{\partial c_i}{\partial x} \quad i = O \text{ and } R \quad (2.120)$$

$$\left. \begin{array}{l} t_2 \geq 0, \quad x \rightarrow \infty \\ t_2 = 0, \quad x \geq 0 \end{array} \right\} \quad c_O = c_O^*, \quad c_R = c_R^* \quad (2.121)$$

$$t_2 > 0, \quad x \geq 0$$

$$D_O \left(\frac{\partial c_O}{\partial x} \right)_{x=0} = -D_R \left(\frac{\partial c_R}{\partial x} \right)_{x=0} \quad (2.122)$$

$$c_O^{s,r} = e^\eta c_R^{s,r} \quad (2.123)$$

where t_1 is the constant time previous to the application of the potential pulse and t_2 the variable pulse time, the total time drop life is $t = t_1 + t_2$, and $c_O^{s,r}$ and $c_R^{s,r}$ are the surface concentrations deduced for a plane electrode given by Eqs. (2.20).

This problem was addressed by Brikmann and Loss [38] and solved later by Galvez and Serna [39]. More recently, a compact expression as a function of the ratio (t_2/t) for the pulse polarographic wave when the two species are initially present in the solution was obtained [40, 41]. Under these conditions, the current can be expressed as

$$I_{NPP}^{DME} = FA(t) \frac{(c_O^* - c_R^* e^\eta)}{1 + \gamma e^\eta} \sqrt{\frac{D_O}{\pi t_2}} h(\alpha) \quad (2.124)$$

with

$$\left. \begin{array}{l} h(\alpha) = \sqrt{\frac{(7/3)\alpha}{1 - (1 - \alpha)^{(7/3)}}} \\ \alpha = \frac{t_2}{t_1 + t_2} \end{array} \right\} \quad (2.125)$$

Note that if $t_1 \rightarrow 0$ (i.e., $t_2 \rightarrow t$ and $\alpha \rightarrow 1$), $h(\alpha) \rightarrow \sqrt{7/3}$ such that Eq. (2.124) presents an ilkovičian behavior (see 2.114):

$$\begin{aligned} I_{NPP}^{DME}(t_1 \rightarrow 0) &= FA_0 t^{2/3} \frac{(c_O^* - c_R^* e^\eta)}{1 + \gamma e^\eta} \sqrt{\frac{D_O}{\pi t}} \sqrt{\frac{7}{3}} \\ &= FA_0 \sqrt{\frac{7D_O}{3\pi}} t^{1/6} \frac{(c_O^* - c_R^* e^\eta)}{1 + \gamma e^\eta} \end{aligned} \quad (2.126)$$

where $A_0 = 4\pi(3m/(4\pi\rho))^{2/3}$.

On the other hand, if $t_2 \ll t_1$ (i.e., $\alpha \rightarrow 0$), $h \rightarrow 1$, Eq. (2.124) transforms into

$$I_{\text{NPP}}^{\text{DME}}(t_2 \ll t_1) = FA \frac{(c_{\text{O}}^* - c_{\text{R}}^* e^{\eta})}{1 + \gamma e^{\eta}} \sqrt{\frac{D_{\text{O}}}{\pi t_2}} \quad (2.127)$$

with $A = A_0 t_1^{2/3}$ being constant. The above equation is simply the current–potential relationship corresponding to a planar electrode with the potential pulse time being t_2 (see Eq. 2.27). Therefore, it presents a cotrellian behavior.

In all the above cases, it is possible to rewrite the current–potential expression as

$$E = E_{1/2}^r + \frac{RT}{F} \ln \left(\frac{I_{\text{d,c}} - I_{\text{NPP}}^{\text{DME}}}{I_{\text{NPP}}^{\text{DME}} - I_{\text{d,a}}} \right) \quad (2.128)$$

which is identical to that obtained in a static planar electrode (see Eq. 2.31).

The sensitivity of NPP is greater than that of dcP because the ratio $I_{\text{NPP}}^{\text{DME}}/I_{\text{dcP}}^{\text{DME}} \cong (3t/7t_2)^{1/2}$ is much greater than unity, provided that $t \gg t_2$. Moreover, the pulse current greatly exceeds the charging current as compared to dc current, since the charging current for a DME is given by [1–3]:

$$I_{\text{c}}^{\text{DME}} = 0.567 C_{\text{i}} (E_{\text{PZC}} - E) m^{2/3} t^{-2/3} \propto t^{-2/3} \quad (2.129)$$

where C_{i} is the integral capacity and E_{PZC} is the potential of zero charge (see Sect. 1.6). Note that C_{i} is given in F cm^{-1} , m in g s^{-1} , E in V, and the current I_{c} in A. So, for NPP it is fulfilled that

$$I_{\text{NPP}}^{\text{DME}} + I_{\text{c}}^{\text{DME}} \propto t^{-1/2} + t^{-2/3} \cong t^{-1/2} \quad (2.130)$$

The NPP current–potential curves calculated from Eq. (2.124) for $t_1 = 1$ s and different values of t_2 have been plotted in Fig. 2.10. As can be seen from these curves, the decrease of the potential pulse time t_2 leads to an increase of the response (and therefore of its sensitivity), whereas it does not affect the location of the current–potential curve.

2.5 Spherical Electrodes

When the electrode does not have macrometric dimensions (i.e., for a radius smaller than 0.05 cm for a time of experiment of 1 s), the geometry becomes fundamental. In this section, special detail will be paid to spherical geometry. The use of spherical electrodes such that the Static Mercury Drop Electrode (SMDE) offers important advantages over solid electrodes on account of its smooth and

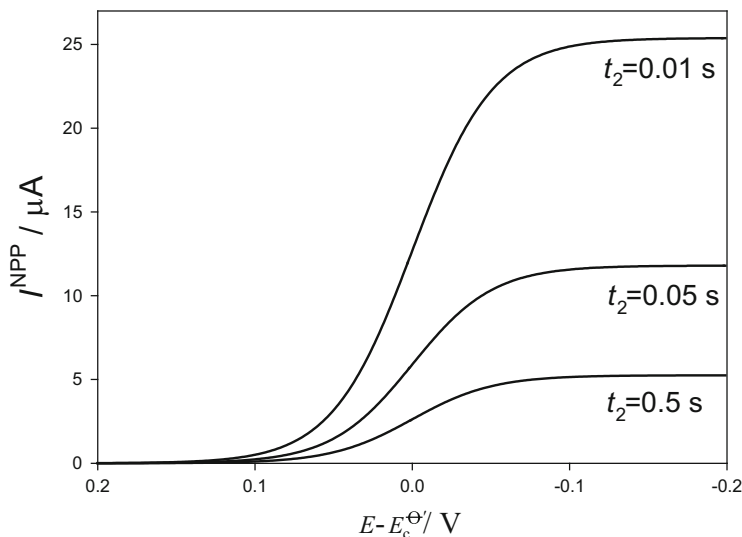


Fig. 2.10 NPP current–potential curves calculated from Eq. (2.124) for a DME with $m = 0.1 \text{ g s}^{-1}$, $D_{\text{O}} = D_{\text{R}} = 10^{-5} \text{ cm}^2 \text{ s}^{-1}$, $c_{\text{O}}^* = 1 \text{ mM}$, $c_{\text{R}}^* = 0$, $t_1 = 1 \text{ s}$, and different values of t_2 indicated in the figure

homogeneous surface and because of the large hydrogen overpotential. This electrode is extensively used in Stripping Analysis by preconcentration of the metal into the small volume of the mercury electrode by cathodic deposition at controlled time and potential [42, 43]. Nowadays gold spherical electrodes and microelectrodes are also widely used [44, 45]. Moreover, the electrode potential can be used to induce uptake or release of species in individual spherical droplets or arrays of droplets and in the monitorization of processes in and around biological cells. In all these examples, the spherical geometry plays an important role [46, 47].

In this section, it will be highlighted that, for nonplanar geometry, finding analytical solutions when the diffusion coefficients of oxidized and reduced species are different is much more complicated than in the planar case, since under these conditions the surface concentrations are time dependent even for reversible processes. However, this situation is of great interest when the ion is transferred between two different phases as in the case of ion transfer between conventional solvents and liquid membranes, or in amalgamation processes. When room temperature ionic liquids (RTILs) are used as solvents, significant differences in the diffusion coefficients of oxidized and reduced species can be also found [48–50], since the electrostatic interactions of the solute with the solvent play an important role in its transport properties, so the different charge of the electroactive species has a significant influence on the magnitude of the diffusion coefficient [49, 51].

2.5.1 Unequal Diffusion Coefficients ($D_O \neq D_R$)

Under these conditions, the diffusion equations to solve are the following:

$$\left. \begin{aligned} \frac{\partial c_O}{\partial t} &= D_O \left(\frac{\partial^2 c_O}{\partial r^2} + \frac{2}{r} \frac{\partial c_O}{\partial r} \right) \\ \frac{\partial c_R}{\partial t} &= D_R \left(\frac{\partial^2 c_R}{\partial r^2} + \frac{2}{r} \frac{\partial c_R}{\partial r} \right) \end{aligned} \right\} \quad (2.131)$$

The boundary value problem (bvp) by considering that the reduced species is initially present in the solution (solution soluble product) or in the electrode (amalgam formation), and that diffusion coefficients of both species are different, is

$$\left. \begin{aligned} t &\geq 0, \quad r \rightarrow \infty \\ t &= 0, \quad r \geq r_s \end{aligned} \right\} \quad c_O = c_O^*, \quad c_R = c_R^* \quad (2.132)$$

for solution soluble product, and

$$\left. \begin{aligned} t &\geq 0, \quad r \rightarrow \infty \\ t &= 0, \quad r \geq r_s \end{aligned} \right\} \quad c_O = c_O^*, \quad c_R = 0 \quad (2.133)$$

$$\left. \begin{aligned} t &\geq 0, \quad r \rightarrow -\infty \\ t &= 0, \quad r \leq r_s \end{aligned} \right\} \quad c_O = 0, \quad c_R = c_R^* \quad (2.134)$$

for amalgam formation

$$t \geq 0, \quad r \geq r_s :$$

$$D_O \left(\frac{\partial c_O}{\partial r} \right)_{r=r_s} = \mp D_R \left(\frac{\partial c_R}{\partial r} \right)_{r=r_s} \quad (2.135)$$

$$c_O^{s, \text{sph}} = e^\eta c_R^{s, \text{sph}} \quad (2.136)$$

with η given by Eq. (2.6) and r_s being the radius of the spherical electrode. In the following and in Eq. (2.135), the upper sign refers to solution soluble product and the lower one to amalgam formation.

By following the procedure indicated in Appendix A, an analytical expression for the current can be deduced:

$$\begin{aligned} \frac{I^{\text{sph}}}{FA_s D_O c_O^*} &= \left(\frac{1 - (c_R^*/c_O^*)e^\eta}{1 + \gamma e^\eta} \right) \left\{ \frac{1}{\sqrt{\pi D_O t}} + \frac{1}{r_s} - \frac{e^\eta \gamma (\gamma \mp 1)}{r_s (\gamma^2 e^\eta \pm 1)} + \right. \\ &\quad \left. + \frac{e^\eta (\gamma \mp 1)^2}{r_s (\gamma^2 e^\eta \pm 1) (1 + \gamma e^\eta)} H(\xi) \right\} \end{aligned} \quad (2.137)$$

with

$$H(\xi) = e^{(\xi/2)^2} \operatorname{erfc}(\xi/2) \quad (2.138)$$

$$\xi = \frac{2\sqrt{D_R t}(\gamma^2 e^\eta \pm 1)}{r_s(1 + \gamma e^\eta)} \quad (2.139)$$

and the time-dependent surface concentrations $c_O^{s,\text{sphe}}$ and $c_R^{s,\text{sphe}}$ are

$$\left. \begin{aligned} c_O^{s,\text{sphe}} &= c_O^{s,r} - \frac{e^\eta \gamma (\gamma \mp 1) (c_O^* - c_O^{s,r})}{(\gamma^2 e^\eta \pm 1)} [H(\xi) - 1] \\ c_R^{s,\text{sphe}} &= c_R^{s,r} + \frac{(\gamma \mp 1) (c_R^* - c_R^{s,r})}{(\gamma^2 e^\eta \pm 1)} [H(\xi) - 1] \end{aligned} \right\} \quad (2.140)$$

$c_O^{s,r}$ and $c_R^{s,r}$ are the time-independent surface concentrations found in planar electrodes (Eq. 2.20), and $A_s = 4\pi r_s^2$.

Note that the finite electrode volume has not been considered to deduce Eq. (2.137), i.e., we have used the so-called Koutecký approximation (see Eq. (2.134) and [52]). Therefore, when amalgamation takes place, these equations with the lower sign cannot be used for very small spherical electrodes for which numerical treatments considering null flux at the center of the electrode are needed.

According to Eq. (2.140), the presence of amalgam has no effect on the voltammetric response of planar electrodes since, under these conditions $r_s \rightarrow \infty$ ($\xi \rightarrow 0$; see Eq. (2.139)) and $H(\xi) \rightarrow 1$ (see also Eq. 2.20).

To obtain Eqs. (2.137) and (2.140), the Dimensionless Parameter Method (DPM) has been used as described in Appendix A and expressions of the concentration profiles have been obtained [52]. In the 1960s, a compact analytical solution for the I - E response was obtained by using the Laplace transform method when the oxidized species was the only present in the electrolytic solution, i.e., for a cathodic wave [53, 54], and non-explicit expressions for the concentration profiles and surface concentrations were obtained.

The time variation of the surface concentration of the oxidized species for different values of γ at a potential corresponding to $E - E_c^{\ominus} = -0.05$ V can be seen in Fig. 2.11. It is clear that for the radii considered the surface concentrations of the oxidized species vary with time for $\gamma < 0.7$ and $\gamma > 1.41$, respectively, while remaining almost constant for other values of γ . It is also observed that the further γ is from the unity, the longer it takes to reach a constant value.

In Fig. 2.12, the analytical current-time curves under anodic and cathodic limiting current conditions calculated from Eq. (2.137) (Fig. 2.12a and b, respectively) when species R is soluble in the electrolytic solution (solid curves) and when species R is amalgamated in the electrode (dotted lines) are plotted. In Fig. 2.12a, the amalgamation effect on the anodic limiting current has been analyzed. As expected, when species R is soluble in the electrolytic solution, the absolute value of the current density increases when the electrode radius decreases because of the enhancement of

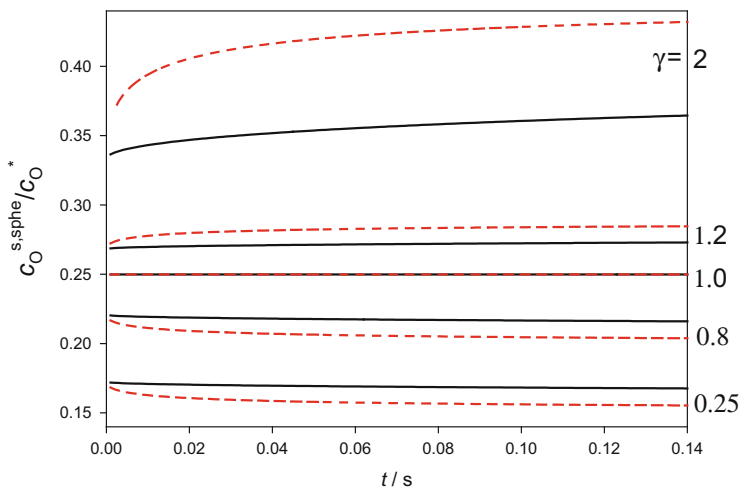


Fig. 2.11 Temporal evolution of the surface concentrations of oxidized species calculated from Eq. (2.140). Two electrode radius values are considered: $r_s = 5 \times 10^{-3}$ cm (solid curves) and $r_s = 5 \times 10^{-4}$ cm (dashed curves), and different γ values indicated in the figure. $E - E_c^\ominus = -0.05$ V, $c_O^* = c_R^* = 1$ mM, $D_O = 10^{-5}$ cm² s⁻¹

the diffusive mass transport. On the other hand, for a given electrode radius the amalgam formation leads to a decrease in the absolute value of the current density, and this decrease is more significant when the electrode radius becomes smaller and/or the electrolysis time is longer. Thus, the radius influence is inverted in relation to the solution soluble product case, so a decrease in electrode radius leads to a decrease in the absolute value of the current density (see Fig. 2.12a, dotted lines). This behavior is due to the diffusion of R taking place inside the spherical electrode. As expected, the cathodic limiting current (see Fig. 2.12b) is not influenced by the amalgam formation, since it is only dependent on the species O behavior.

The analytical equations obtained allow us to study the anodic–cathodic wave. The current–potential curves for $\gamma = 0.7$ are plotted in Fig. 2.13 for three values of the electrode radius and for two different initial conditions: when species O is the only one present (Fig. 2.13a), and when both species are present in the system (Fig. 2.13b).

In the first case, when only species O is initially present in the electrolytic solution (Fig. 2.13a), it is observed that the amalgamation of species R leads to a shift of the wave to more negative potential values, and this shift is greater the more spherical the electrode, i.e., when the duration of the experiment increases or the electrode radius decreases. In the second case (Fig. 2.13b), both species are initially present in the system so we can study the anodic–cathodic wave. In the anodic branch of the wave, the amalgamation produces a decrease in the absolute value of the current. As is to be expected, the null current potential, crossing potential, or equilibrium potential (E_{Eq}) is not affected by the diffusion rates (D_O and D_R), by the electrolysis time, by the electrode geometry (r_s), nor by the behavior of species R

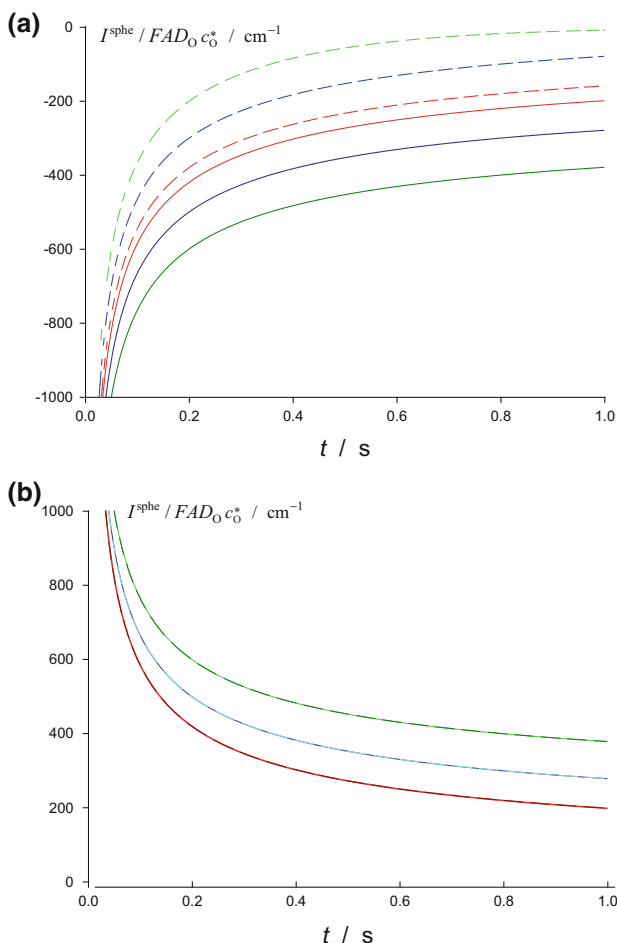


Fig. 2.12 Influence of the electrode radius on the current–time curves under anodic (a) and cathodic (b) limiting conditions (Eq. 2.137) when species R is soluble in the electrolytic solution (solid curves) and when it is amalgamated in the electrode (dashed curves). The electrode radius values (in cm) are: $r_s = 5 \times 10^{-2}$ (red curves), $r_s = 10^{-2}$ (blue curves), and $r_s = 5 \times 10^{-3}$ (green curves). $c_O^* = c_R^* = 1 \text{ mM}$, $D_O = D_R = 10^{-5} \text{ cm}^2 \text{ s}^{-1}$. (The dashed green curve has been calculated numerically for $t > 0.5 \text{ s}$). Reproduced with permission [52]

(soluble in the electrolytic solution or in the electrode) (see Eq. 2.33). On the other hand, the half-wave reversible potential is affected by the diffusional behavior of species O and R and the following is observed for a solution soluble product:

$$E_{1/2}^r \Big|_{\text{sphe}} \begin{matrix} \geq \\ \leq \end{matrix} E_{1/2}^r \Big|_{\text{plane}} \quad \text{if} \quad \gamma \begin{matrix} \leq \\ > \end{matrix} 1 \quad (2.141)$$

Note that in this case the determination of the half-wave potential can be made by fitting experimental data to the Eq. (2.137) since Eq. (2.31) is not fulfilled under

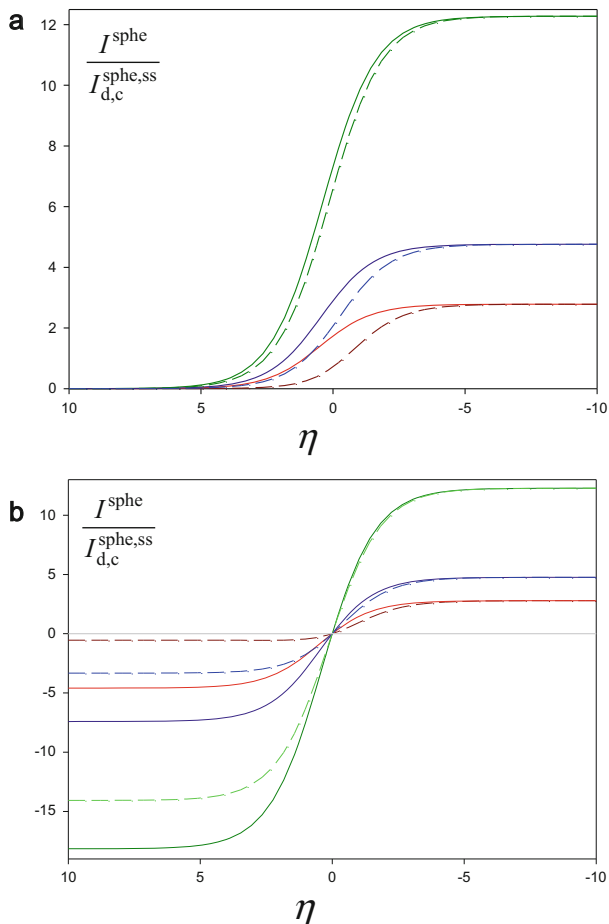


Fig. 2.13 Influence of the c_R^*/c_O^* ratio on the anodic-cathodic waves when species R is soluble in the electrolytic solution (*solid curves*) (Eq. (2.137) considering the upper sign) and when it is amalgamated in the electrode (*dotted curves*) (Eq. (2.137) considering the lower sign). $I_{d,c}^{\text{sphe,ss}} = FA_s D_O c_O^* / r_s$ (see Eq. 2.148). Three electrode sphericity values ($\sqrt{D_R t} / r_s$) are considered: 0.071 (*green curves*), 0.214 (*blue curves*), and 0.451 (*red curves*), and two different initial concentration ratios: $c_O^* = 1 \text{ mM}$, $c_R^* = 0$ (**a**), $c_O^* = c_R^* = 1 \text{ mM}$ (**b**). $D_O = 10^{-5} \text{ cm}^2 \text{ s}^{-1}$, $\gamma = 0.7$. Reproduced with permission [52]

these conditions and the plots E vs. $\ln \left(\left(I_{d,c}^{\text{sphe}} - I^{\text{sphe}} \right) / \left(I^{\text{sphe}} - I_{d,a}^{\text{sphe}} \right) \right)$ cannot be used as in the case of planar electrodes. This is because under the above conditions the current presents a complex expression which cannot be written as the product of a function of the potential by a function of time, as in the case of the electrodes mentioned above.

2.5.2 Equal Diffusion Coefficients ($D_O = D_R$)

When both diffusion coefficients are equal ($D_O = D_R = D$), and both species are soluble in the electrolytic solution (taking only the upper sign in Eq. (2.135)), Eqs. (2.137) and (2.140) drastically simplify to the following [1–4, 40, 41, 55, 56]:

$$\frac{I^{\text{sphe}}}{FA_s D c_O^*} = \left(\frac{1 - (c_R^*/c_O^*)e^\eta}{1 + e^\eta} \right) \left\{ \frac{1}{\sqrt{\pi D t}} + \frac{1}{r_s} \right\} \quad (2.142)$$

$$\left. \begin{aligned} c_O^{\text{s,sphe}} \Big|_{r=1} &= c_O^{\text{s,r}} \Big|_{r=1} = \frac{e^\eta (c_O^* + c_R^*)}{1 + e^\eta} \\ c_R^{\text{s,sphe}} \Big|_{r=1} &= c_R^{\text{s,r}} \Big|_{r=1} = \frac{c_O^* + c_R^*}{1 + e^\eta} \end{aligned} \right\} \quad (2.143)$$

and the concentration profiles are given by the following equations:

$$\left. \begin{aligned} c_O(r, t) &= c_O^* + \frac{r_s}{r} (c_O^{\text{s,r}} - c_O^*) \operatorname{erfc} \left(\frac{r - r_s}{2\sqrt{Dt}} \right) \\ c_R(r, t) &= c_R^* + \frac{r_s}{r} (c_R^{\text{s,r}} - c_R^*) \operatorname{erfc} \left(\frac{r - r_s}{2\sqrt{Dt}} \right) \end{aligned} \right\} \quad (2.144)$$

Appendix B describes in detail the solution of this problem as an application of the Laplace's Transform method and Eqs. (2.142)–(2.144) have also been deduced.

As can be inferred from Eq. (2.143), under these conditions the surface concentrations of both species are time independent, so the current given by Eq. (2.142) can be written as

$$\begin{aligned} I^{\text{sphe}} &= FA_s D_O (c_O^* - c_O^{\text{s,r}}) \left\{ \frac{1}{\sqrt{\pi D t}} + \frac{1}{r_s} \right\} \\ &= -FA_s D_R (c_R^* - c_R^{\text{s,r}}) \left\{ \frac{1}{\sqrt{\pi D t}} + \frac{1}{r_s} \right\} \end{aligned} \quad (2.145)$$

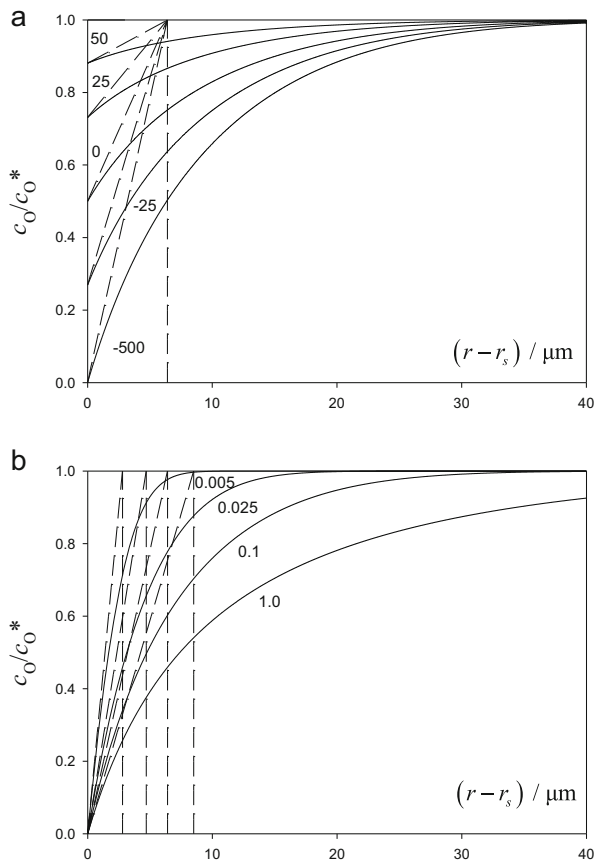
From Eq. (2.145), it is clear that the diffusion layer thickness in spherical diffusion is (compare Eqs. (2.145) and (2.26)) [12],

$$\delta_{\text{sphe}}^r = \frac{1}{\left\{ \frac{1}{\sqrt{\pi D t}} + \frac{1}{r_s} \right\}} \quad (2.146)$$

which is independent of the applied potential, as in the case of planar diffusion.

In Fig. 2.14 we have plotted the transient accurate concentration profiles for species O, $c_O(r, t)$ (Eq. 2.144) and the linear concentration profiles $\left(c_O(r, t) = \frac{c_O^* - c_O^{\text{s,r}}}{\delta_{\text{sphe}}^r} (r - r_s) + c_O^{\text{s,r}} \right)$ at a fixed time and different potentials (Fig. 2.14a), and at a fixed potential and different times (Fig. 2.14b).

Fig. 2.14 Concentration profiles of a spherical electrode for the application of a potential pulse for different values of $(E - E_c^{\ominus'})$ (in mV) for a fixed time (a), and different values of time (in s) for a fixed potential (b), shown in the curves. $D_O = D_R = D$. The electrode radius is $10\text{ }\mu\text{m}$. Dashed lines correspond to their linear concentration profiles. $t = 0.1\text{ s}$ (a) and $(E - E_c^{\ominus'}) = -500\text{ mV}$ (b). Reproduced with permission [12]



When compared with the linear concentration profiles of Fig. 2.1a, it can be observed that, in agreement with Eq. (2.146) for spherical electrodes, the Nernst diffusion layer is, under these conditions, independent of the potential in all the cases. As for the time dependence of the profiles shown in Fig. 2.14b, it can be seen that the Nernst diffusion layer becomes more similar to the electrode size at larger times. Analogous behavior can be observed when the electrode radius decreases.

Expressions for the cathodic and anodic limiting currents can also be easily obtained for spherical electrodes by making $e^\eta \rightarrow 0$ and $e^\eta \rightarrow \infty$ in Eq. (2.142),

$$\left. \begin{aligned} I_{d,c}^{\text{sph}} &= FA_s D c_O^* \left(\frac{1}{\sqrt{\pi D t}} + \frac{1}{r_s} \right) \\ I_{d,a}^{\text{sph}} &= -FA_s D c_R^* \left(\frac{1}{\sqrt{\pi D t}} + \frac{1}{r_s} \right) \end{aligned} \right\} \quad (2.147)$$

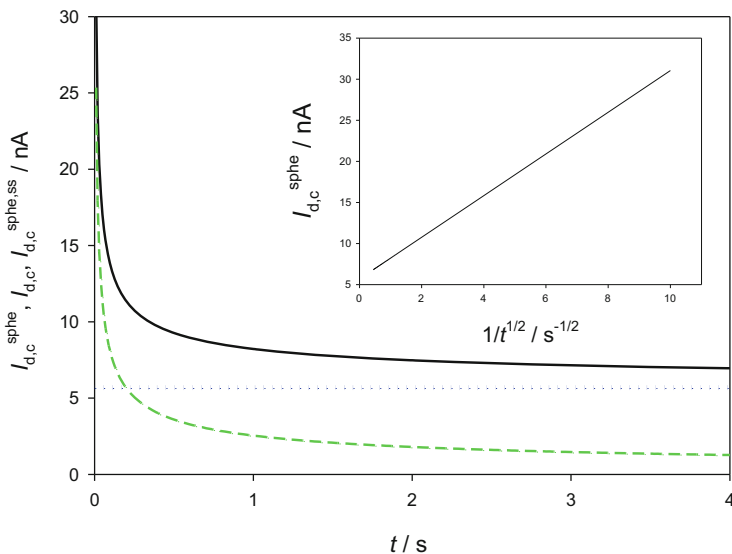


Fig. 2.15 (Solid line) Current–time curves for the application of a constant potential to a spherical electrode calculated from Eq. (2.142). $D_O = D_R = 10^{-5} \text{ cm}^2 \text{ s}^{-1}$, $c_O^* = c_R^* = 1 \text{ mM}$, $r_s = 0.001 \text{ cm}$, $(E - E_c^{\ominus}) = -0.2 \text{ V}$, $T = 298 \text{ K}$. (Dashed line) Current–time curves for the application of a constant potential to a planar electrode of the same area as the spherical one calculated from Eq. (2.28). (Dotted line) Steady-state limiting current for a spherical electrode calculated from Eq. (2.148). The inner figure corresponds to the plot of the current of the spherical electrode versus $1/\sqrt{t}$

The time evolution of the cathodic limiting current (Eq. 2.147) has been plotted in Fig. 2.15 together with that obtained for a planar electrode (Eq. 2.28) and the constant steady-state limiting current for a spherical electrode given by

$$I_{d,c}^{\text{sphe,ss}} = FA_s D c_O^* \frac{1}{r_s} \quad (2.148)$$

From this figure, it can be seen that the current decays with time as in the planar case although this decrease leads to a constant value, $I_{d,c}^{\text{sphe,ss}}$, different from zero, which will be achieved sooner as the electrode radius diminishes. The current for times close to zero is identical to that obtained in a planar electrode given to the prevalence of the term $1/\sqrt{\pi D t}$ over the inverse of the radius. For longer times, the opposite happens and the term $1/r_s$ is dominant.

In order to obtain values for the diffusion coefficient at spherical electrodes, a logarithmic plot of the current versus time would lead to nonlinear dependence (see Eq. 2.147). In this case a plot of the current versus $1/\sqrt{t}$ is more appropriate (see inner curve in Fig. 2.15) and this plot also allows the determination of the electrode radius by combining the values of the slope ($FA_s c_O^* \sqrt{D/\pi}$) and intercept ($FA_s D c_O^*/r_s$).

Finally, from Eq. (2.145), it is clear that the half-wave potential, which under these conditions ($D_O = D_R$) coincides with the formal potential $E_c^{\ominus'}$, can be easily

obtained from the linear analysis of the potential versus $\ln\left(\left(I_{d,c}^{\text{sphe}} - I^{\text{sphe}}\right)/\left(I^{\text{sphe}} - I_{d,a}^{\text{sphe}}\right)\right)$ curves like in the case of a planar electrode or a DME with the expanding plane model since, as in these cases, the current presents the potential and time dependences in separate terms.

2.6 Other Electrodes Geometries

This section addresses other electrode geometries, both uniformly accessible (like cylindrical electrodes) and non-uniformly accessible (like discs and bands) (see Scheme 2.4). Cylindrical electrodes are the best example of electrodes where one dimension (the radius) is much smaller than the other (the length). Under these conditions, edge effects on the current can be considered as negligible and diffusion is mainly radial and therefore only dependent on the distance r to the center of the cylinder [10]. In relation with disc and band electrodes, it is important to highlight that the mass transport of species in solution requires a much more complex mathematical treatment due to their nonuniform accessibility. The theoretical modeling of the mass transport at these electrodes shows that the current is an average quantity resulting from an average mass flux over the electrode surface [10, 57, 58]. Hence, in the case of disc electrodes, depending on the electrode size, the current will be the result of mixed mass transport, with a predominant component that could change from linear (large sizes or short times) to radial (small sizes or long times). This nonuniform accessibility leads to more efficient mass transport to the electrode edge and to a shielding effect of this at the center of the electrode (see Fig. 2.16). Even so, this electrode remains the most popular and practical due to its easy manufacture in a wide range of sizes, and the easy and controlled cleaning of its surface [58, 59].

For the sake of simplicity only electrode processes in which the oxidized and reduced species are soluble in the electrolytic solution and have equal diffusion coefficients will be considered.

Under these conditions, the differential equation systems for the diffusion mass transport of species O and R is given by

$$\left. \begin{aligned} \frac{\partial c_O}{\partial t} &= D \nabla^2 c_O \\ \frac{\partial c_R}{\partial t} &= D \nabla^2 c_R \end{aligned} \right\} \quad (2.149)$$

where ∇^2 is the Laplacian operator given by any equation of Table 2.2. When the flux is conserved in the electrode surface, the following solution for the sum of concentrations of species O and R is obtained (see Appendix in reference [60]):

$$c_O(q, t) + c_R(q, t) = c_O^* + c_R^* \quad (2.150)$$

Scheme 2.4 Most common electrode and microelectrode geometries and their diffusion fields

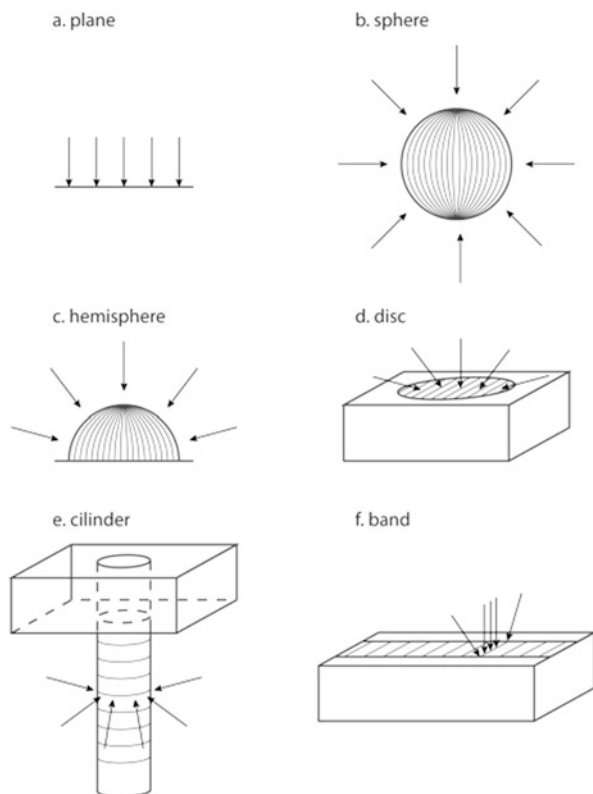


Fig. 2.16 Evolution of the normalized flux at $z = 0$, $J_N = (\partial c_i / \partial z)_{z=0} / (2c_i^* / \pi r_d)$ versus (r/r_d) for a disc electrode calculated from Eq. (C.18) of Appendix C (see Scheme 2.5)

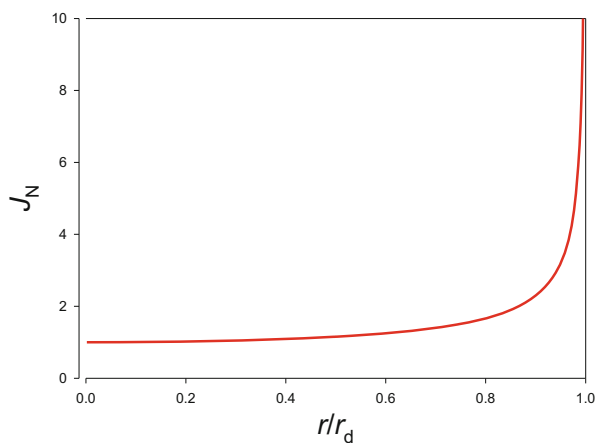


Table 2.2 Expressions for the diffusion mass transport operators given by Fick's second law

Electrode geometry	Laplacian operator ∇^2
Planar	$\left(\frac{\partial^2}{\partial x^2}\right)$
Spherical	$\left(\frac{\partial^2}{\partial r^2} + \frac{2}{r} \frac{\partial}{\partial r}\right)$
Cylindrical	$\left(\frac{\partial^2}{\partial r^2} + \frac{1}{r} \frac{\partial}{\partial r}\right)$
Band	$\left(\frac{\partial^2}{\partial x^2} + \frac{\partial^2}{\partial z^2}\right)$
Disc	$\left(\frac{\partial^2}{\partial r^2} + \frac{1}{r} \frac{\partial}{\partial r} + \frac{\partial^2}{\partial z^2}\right)$

with q and t referring to spatial coordinates and time values, respectively. Equation (2.150) is, of course, fulfilled at the electrode surface, i.e., for $q = q^s$, with q^s being the coordinates at the surface of the electrode.⁵ For nernstian processes, at q^s :

$$c_{\text{O}}^{s,r} = e^{\eta} c_{\text{R}}^{s,r} \quad (2.151)$$

The combination of Eqs. (2.150) and (2.151) transforms the problem of two variables c_{O} and c_{R} into two separate problems of only one variable with constant surface conditions,

$$\left. \begin{array}{l} \frac{\partial c_{\text{O}}}{\partial t} = D \nabla^2 c_{\text{O}} \\ \left. \begin{array}{l} t \geq 0, q \rightarrow \infty \\ t = 0, q \geq q^s \end{array} \right\} c_{\text{O}}(q, t) = c_{\text{O}}^* \\ t \geq 0, q = q^s \quad c_{\text{O}}^{s,r} = \frac{e^{\eta} (c_{\text{O}}^* + c_{\text{R}}^*)}{1 + e^{\eta}} \end{array} \right\} \quad (2.152)$$

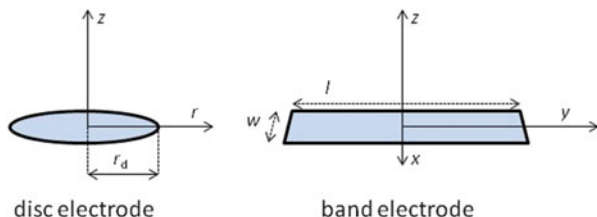
$$\left. \begin{array}{l} \frac{\partial c_{\text{R}}}{\partial t} = D \nabla^2 c_{\text{R}} \\ \left. \begin{array}{l} t \geq 0, q \rightarrow \infty \\ t = 0, q \geq q^s \end{array} \right\} c_{\text{R}}(q, t) = c_{\text{R}}^* \\ t \geq 0, q = q^s \quad c_{\text{R}}^{s,r} = \frac{(c_{\text{O}}^* + c_{\text{R}}^*)}{1 + e^{\eta}} \end{array} \right\} \quad (2.153)$$

with η being given in Eq. (2.6).

The two diffusional problems above are very similar to those corresponding to a process under limiting current conditions but with $c_{\text{O}}^{s,r} \neq 0$ and/or $c_{\text{R}}^{s,r} \neq 0$.

⁵ For a cartesian set of coordinates, like those used for band electrodes, q denotes coordinates x , y , and z , whereas for a cylindrical set of coordinates, like those corresponding to disc electrodes, q denotes coordinates r and z . In both cases, q^s refers to $z = 0$.

Scheme 2.5 Disc and band electrodes and relevant coordinates for each geometry (disc area, $A_d = \pi r_d^2$; band area, $A_b = wl$)



Note that at uniformly accessible electrodes, spheres and cylinders, the mass flux is identical at all the points of its surface, whereas at non-uniformly accessible ones, discs and bands, the mass flux varies through the radius and the width, respectively. Therefore, in these cases, the surface gradient should be calculated by integrating the flux over the electrode surface such that the current is given by (see Scheme 2.5):

$$\frac{I^{\text{disc}}}{F} = 2A_d D c_O^* \frac{1}{r_d} \int_{R=0}^{R=1} \left(\frac{\partial C_O}{\partial Z} \right)_{z=0} R dR \quad (2.154)$$

$$\frac{I^{\text{band}}}{F} = 2A_b D c_O^* \frac{1}{w} \int_{X=0}^{X=1/2} \left(\frac{\partial C_O}{\partial Z} \right)_{z=0} dX \quad (2.155)$$

with $C_O = c_O/c_O^*$, $R = r/r_d$, $X = x/w$ and $Z = z/r_d$ (disc) or $Z = z/w$ (band).

It has been verified that the current obtained when a potential step is applied only differs from the corresponding to the limiting cathodic or anodic currents in the constant terms $(c_O^* - c_O^{s,r})$ and $(c_R^* - c_R^{s,r})$ instead of c_O^* and c_R^* , respectively (with $c_i^{s,r}$ being the surface concentration of species i). From Eqs. (2.152) and (2.153), the surface concentrations are independent of the electrode geometrical characteristics under Nernstian conditions [60]. Hence, the average current can be expressed independently of the electrode geometry as the product of a function of the applied potential $(c_O^* - c_O^{s,r})$ and a function of time and the electrode geometry $f_G(t, q_G)$ (with q_G being the characteristic dimension of the electrode), which is given in Table 2.3 for each particular geometry:

$$\begin{aligned} I^G &= F A_G D \times (c_O^* - c_O^{s,r}) \times f_G(t, q_G) = \\ &= -F A_G D \times (c_R^* - c_R^{s,r}) \times f_G(t, q_G) \end{aligned} \quad (2.156)$$

with

$$c_O^* - c_O^{s,r} = -(c_R^* - c_R^{s,r}) = \frac{c_O^* - e^\eta c_R^*}{1 + e^\eta} \quad (2.157)$$

where A_G is the electrode area and q_G the characteristic dimension of the electrode (Table 2.3).

The cathodic and anodic limiting currents for an electrode of a given geometry can be obtained by imposing $\eta \rightarrow \mp\infty$ on (2.156) and (2.157)

Table 2.3 Expressions for functions $f_G(t, q_G)$ and $f_{G,\text{micro}}$ for the four electrode geometries considered. $q_G = r_d$ for discs; $q_G = r_s$ for spheres or hemispheres; $q_G = r_c$ for cylinders; and $q_G = w$ for bands. Note that functions $f_G(t, q_G)$ and $f_{G,\text{micro}}$ have dimensions of 1/length

Electrode	Function $f_G(t, q_G)$	$f_{G,\text{micro}}$
Disc (radius r_d , Area $A_d = \pi r_d^2$)	$\frac{4}{\pi} \frac{1}{r_d} \left(0.7854 + 0.44315 \frac{r_d}{\sqrt{Dt}} + 0.2146 \exp \left(-0.39115 \frac{r_d}{\sqrt{Dt}} \right) \right)$	$\frac{4}{\pi} \frac{1}{r_d}$
Sphere (radius r_s , $A_s = 4\pi r_s^2$)	$\frac{1}{r_s} + \frac{1}{\sqrt{\pi Dt}}$	$\frac{1}{r_s}$
Band (height w , length l , $A_b = wl$)	$\frac{1}{w} + \frac{1}{\sqrt{\pi Dt}}$ if $Dt/w^2 < 0.4$ $0.25 \sqrt{\frac{\pi}{Dt}} \exp \left(-0.4 \frac{\sqrt{\pi Dt}}{w} \right) + \frac{\pi}{w \ln \left(5.2945 + 5.9944 \frac{\sqrt{Dt}}{w} \right)}$ if $Dt/w^2 \geq 0.4$	$\frac{1}{w} \frac{2\pi}{\ln[64Dt/w^2]}$
Cylinder (radius r_c , length l , $A_c = 2\pi r_c l$)	$\frac{1}{\sqrt{\pi Dt}} \exp \left(-0.1 \frac{\sqrt{\pi Dt}}{r_c} \right) + \frac{1}{r_c \ln \left(5.2945 + 1.4986 \frac{\sqrt{Dt}}{r_c} \right)}$	$\frac{1}{r_c} \frac{2}{\ln[4Dt/r_c^2]}$

$$\left. \begin{aligned} I_{d,c}^G &= F A_G D \times c_O^* \times f_G(t, q_G) \\ I_{d,a}^G &= -F A_G D \times c_R^* \times f_G(t, q_G) \end{aligned} \right\} \quad (2.158)$$

In order to highlight the non-uniformity of the concentration distribution around the disc, Fig. 2.17 shows the concentration profiles of oxidized species corresponding to the application of a potential step to a disc electrode for three values of r_d (500, 50, and 5 μm), and two values of the applied potential ($E = E_c^{\ominus'}$ and an E value corresponding to limiting current) for a time $t = 0.5$ s. From this figure, it can be deduced that, although the concentration profiles are logically affected by the applied potential, the Nernst diffusion layer thicknesses are independent of it. It can also be observed from this figure that the solution region adjacent to the electrode surface disturbed by the mass transport is much lower than the disc radius for higher values of r_d . Moreover, in this case (see curves with $r_d = 500$ μm in Fig. 2.17a and b), the dominant mass transport is that corresponding to planar diffusion, i.e., practically all the flux at the surface takes place at the normal coordinate z , with the exception of r values close to the edge of the disc. This gives rise to a planar front for δ_d , as seen in Fig. 2.17a and b. As the disc radius decreases (see Fig. 2.17c–f), the linear diffusion layer thickness becomes comparable to or even higher than r_d , showing a continuous variation between the center and the edge of the disc. For a radius $r_d = 5$ μm (see Fig. 2.17e and f), the radial mass transport becomes dominant in the whole response.

A consequence of the temporal independence of the surface concentrations is that under transient conditions, the relation $I^G/I_{d,c}^G$ and the curve $E/$

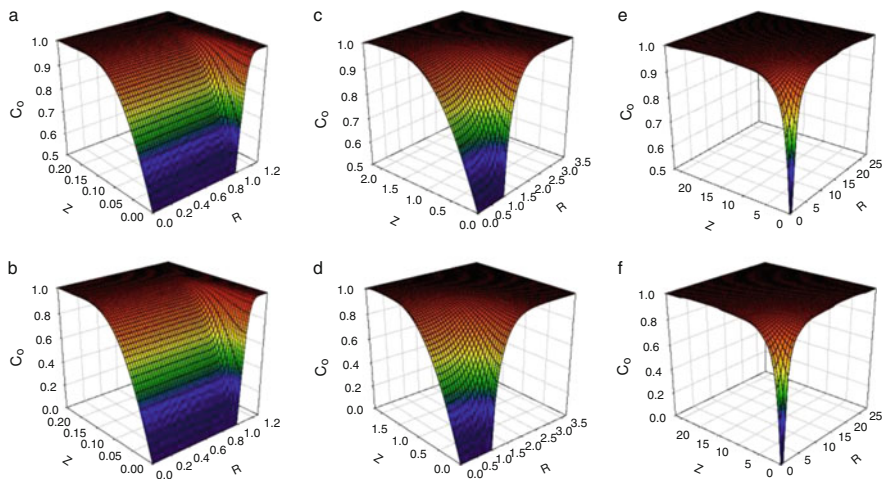


Fig. 2.17 Concentration profiles of oxidized species in reaction Scheme (1) corresponding to the application of a potential step to a disc electrode for three values of r_d (μm): 500 (a, b), 50 (c, d), and 5 (e, f), and two values of the applied potential: $E = E_c^{\Theta'}$ (a, c, and e) and $E = E_c^{\Theta'} - 0.256$ V (b, d, and f). $C_O = c_O/c_O^*$, $R = r/r_d$, and $Z = z/r_d$. These profiles have been numerically obtained by following the procedure described in reference [61] for a time $t = 0.5$ s and $D_O = D_R = 10^{-5}$ $\text{cm}^2 \text{s}^{-1}$. $T = 298.15$ K. Reproduced with permission [59]

$\ln((I_{d,c}^G - I^G)/(I^G - I_{d,a}^G))$ at a fixed time are independent of the electrode geometry,

$$\frac{I^G}{I_{d,c}^G} = \frac{1 - e^{\eta}(c_R^*/c_O^*)}{1 + e^{\eta}} \quad (2.159)$$

or,

$$E - E_c^{\Theta'} = \frac{RT}{F} \ln \left(\frac{I_{d,c}^G - I^G}{I^G - I_{d,a}^G} \right) \quad (2.160)$$

The analysis of the current–time curves at electrodes or microelectrodes of different geometries has also a great interest in detecting the presence of small particles or nanoparticles at its surface or even single nanoparticles events through the current due to the electro-oxidation (or reduction) of the particles (see Fig. 2.18) or to an electrocatalytic reaction on the nanoparticle surface when this comes into contact with the electrode and transiently sticks to it [62–65].

In Fig. 2.19, we have plotted the $(I^G/I_{d,c}^G) - (E - E_c^{\Theta'})$ curves for discs, spheres, bands, and cylinders calculated from Eqs. (2.156) and (2.159) when both species are initially present in the solution in order to show that, for a given process, this ratio is independent of the size and geometry of the electrode considered and independent of the transient or stationary character of the response. On the basis of

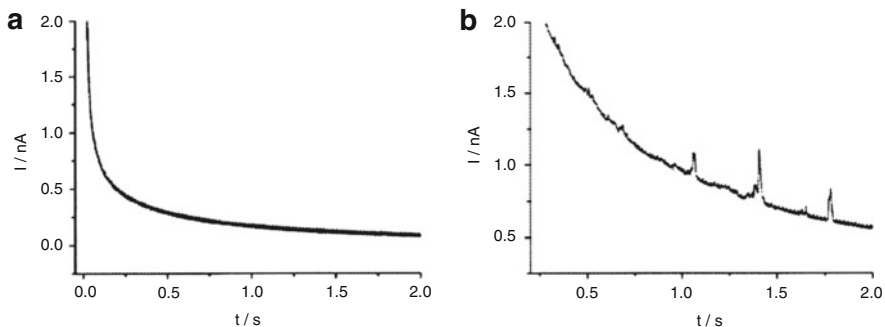


Fig. 2.18 Chronoamperometric profiles showing oxidative faradaic transients of gold nanoparticles at potentials of (a) 0.8 V and (b) 1.1 V at a Glassy Carbon microelectrode of 11 μm of radius. Reproduced from reference [62] with permission

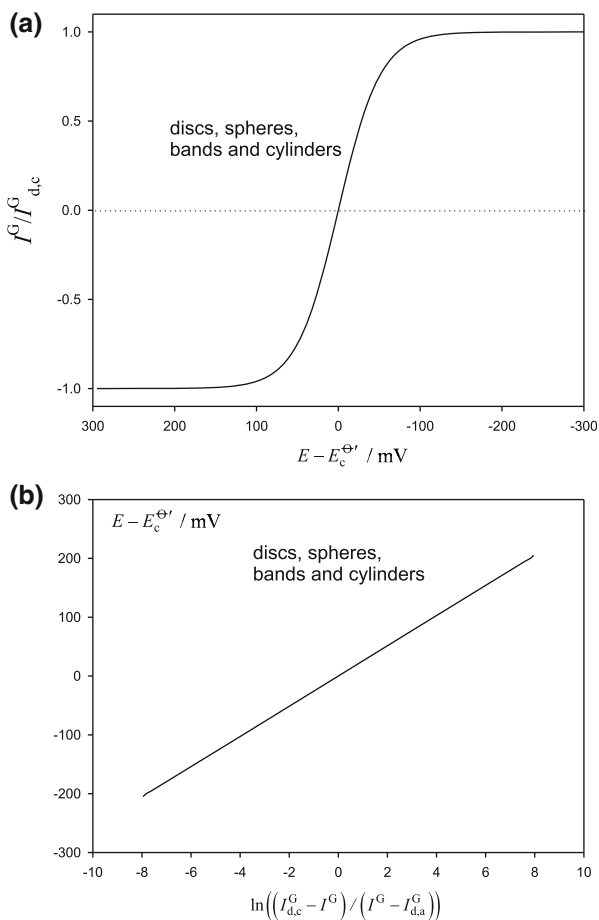


Fig. 2.19 (a) $(I^G/I_{d,c}^G) - (E - E_c^{\ominus'})$ curves and (b) $(E - E_c^{\ominus'}) - \ln((I_{d,c}^G - I^G)/(I^G - I_{d,a}^G))$ for discs, spheres, bands, and cylinders calculated from Eqs. (2.159) and (2.160) when both species are initially present in the solution and $c_R^*/c_O^* = 1$

these results, it is clear that the analysis of the curve $E/\ln((I_{d,c}^G - I^G)/(I^G - I_{d,a}^G))$ is identical to that carried out in the case of planar or spherical electrodes (see for example Eq. 2.31). So, whatever the geometry considered, by combining Eq. (2.156) and

$$I^G = FA_G D \left(\frac{\partial c_O}{\partial q_N} \right)_{q^s} \quad (2.161)$$

with q_N being the normal coordinate value at the electrode surface, the Nernst diffusion layer δ_G^r is easily determined as a function of time, size, and geometry (compare Eq. (2.156) with Eqs. (2.26) and (2.145)):

$$\delta_G^r = \frac{c_O^* - c_O^{s,r}}{I^G / FA_G D c_O^*} = \frac{1}{f_G(t, q_G)} \quad (2.162)$$

with $f_G(t, q_G)$ given in Table 2.3.

Note that if the electrode is not uniformly accessible such as disc and band electrodes, the diffusion layer thickness given by Eq. (2.162) has an average character [59], and in this case it will be denoted $\bar{\delta}_G^r$.

The temporal evolution of $\bar{\delta}_{disc}^r(t)$ and $\bar{\delta}_{band}^r(t)$, calculated from Eq. (2.162) and Table 2.3 for disc (solid lines) and band (solid-dotted lines) electrodes of three sizes ($r_0 = 500, 50$, and $5 \mu\text{m}$, with r_0 being equal to r_d or $w/2$, respectively), has been plotted in Fig. 2.20. We have compared these curves with those obtained for spherical (dashed lines) and cylindrical (dotted lines) electrodes considering $r_d = r_s = r_c$ (with $\delta_{sph}^r(t)$ and $\delta_{cyl}^r(t)$ being calculated from equations in Table 2.3).

From these curves it can be seen that the Nernst diffusion layer, δ_G^r , increases with time in all cases. Moreover, Fig. 2.20a shows how these curves are all coincident at short times and only small differences appear between the couples “bands and cylinders” and “spheres and discs” at times longer than 0.2 s. This indicates that for this electrode size and time below 0.2 s, the prevalent diffusion field is planar, so the electrode geometry becomes irrelevant. As the electrode size decreases (Fig. 2.20b and c), so does the temporal dependence of δ_G^r and the different curves begin to separate until they reach a steady state in the case of discs and spheres, or a pseudo-steady state in the case of bands and cylinders (Fig. 2.20c). Note that the ratio between the diffusion layers corresponding to small discs and spheres $\delta_{disc}^{r,micro}$ and $\delta_{sph}^{r,micro}$ tends to the value $\pi/4$ (see also Sect. 2.7).

It is worth highlighting that, when different diffusion coefficients are considered, the half-wave potential depends on the characteristics of the diffusive field (geometry and size of the electrode), as indicated in Sect. 2.5.1. The variation of the half-wave potential $E_r^{1/2}$ with the electrode radius for cylindrical and spherical electrodes for $\gamma = 3$ (numerically calculated) has been plotted in Fig. 2.21. The

Fig. 2.20 Temporal evolution of $\bar{\delta}_{\text{disc}}^r(t)$ and $\bar{\delta}_{\text{band}}^r(t)$, calculated from equations in Table 2.3 for disc (*solid lines*) and band (*solid-dotted lines*) electrodes of three sizes ($r_0 = 500, 50$, and $5 \mu\text{m}$, with r_0 being equal to r_d or $w/2$). These curves have been compared with those obtained for spherical (*dashed lines*) and cylindrical (*dotted lines*) electrodes considering $r_d = r_s = r_c$ (with $\delta_{\text{sph}}^r(t)$ and $\delta_{\text{cyl}}^r(t)$ is calculated from equations in Table 2.3). Reproduced with permission [59]

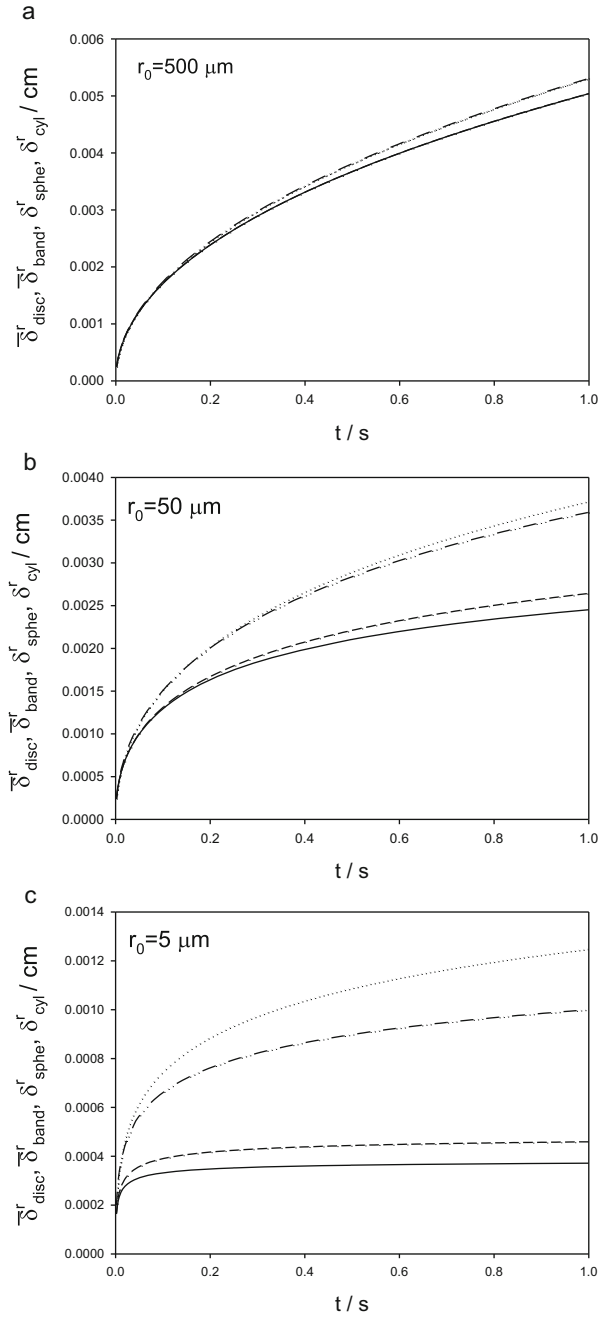
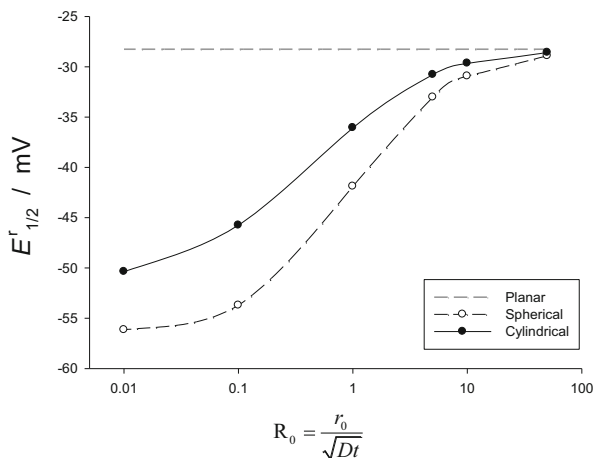


Fig. 2.21 Evolution of the half-wave potential with the electrode size for spherical (white dots) and cylindrical (black dots) electrodes. The value of $E_{1/2}^r$ for a planar electrode has been included for comparison (dashed line). $r_0 = r_s$ for a spherical electrode and $r_0 = r_c$ for a cylindrical one. $D_O = 10^{-5} \text{ cm}^2 \text{ s}^{-1}$, $\gamma = \sqrt{D_O/D_R} = 3$



half-wave potential of planar electrodes is also shown for comparison. As can be seen, the stationary value of $E_{1/2}^r = E_c^{\ominus'} + (RT/F)\ln(1/\gamma^2)$ (see Appendix C and Eq. (2.167)) is reached for spherical electrodes for values of $R_0 = 0.01$, whereas for cylindrical ones a steady-state value is not reached.

2.7 Microelectrodes. Steady-State Voltammetry

A microelectrode is usually defined as an electrode with at least one characteristic dimension (r_G) on the micrometer scale (of tens of micrometers or less). As is well known, the progressive decreasing of the electrode size produces an enhancement of the mass transport between the electrode surface and the bulk of the solution. This leads to important advantages in electrochemistry like fast establishment of stationary response (i.e., independent of time), improved ratio of faradaic to charging currents, decrease of the ohmic drop, short response times, and others derived from its small size: electroanalytical measurements in living organisms, microscopic sensors and arrays, among others. The currents observed at microelectrodes typically lie in the pA to nA range, and are much smaller than those measured with conventional electrodes of millimetric dimensions. It is only since the 1980s that very small electrodes and appropriate instruments to measure such low currents accurately have been available (see [9, 66, 67]). The scarce ohmic drop permits the study of electrochemical processes in high resistance solvents, low supported solutions, solids, and gases. Moreover, the effect of convective flux on mass transport is greatly reduced because the rate of diffusional transport can be several orders of magnitude larger than that attainable at a macro or planar electrode and other modes of transport are masked by the large diffusional contribution. More recently, nanoelectrodes have been developed with their characteristic dimension of a few tens of nanometers, which is comparable to the diffuse double-layer thickness. This can lead to deviations from the classic voltammetric theory [68, 69].

In this section, we will show that the stationary responses obtained at microelectrodes are independent of whether the electrochemical technique employed was under controlled potential conditions or under controlled current conditions, and therefore, they show a universal behavior. In other words, the time independence of the I/E curves yields unique responses independently of whether they were obtained from a voltammetric experiment (by applying any variable on time potential), or from chronopotentiometry (by applying any variable on time current). Hence, the equations presented in this section are applicable to any multipotential step or sweep technique such as Staircase Voltammetry or Cyclic Voltammetry.

Special attention should be paid to spherical geometry, since the mathematical treatment of spherical microelectrodes is the simplest and exemplifies very well the attainment of the steady state observed at microelectrodes of more complex shapes. Indeed, spherical or hemispherical microelectrodes, although difficult to manufacture, are the paragon of mathematical model for diffusion at microelectrodes, to the point that the behavior of other geometries is always compared against them.

The expression for the current of a reversible electrode process corresponding to a microelectrode of a given geometry will be deduced from Eq. (2.156) by making $q_G \ll \sqrt{\pi Dt}$. Under these conditions, a stationary current–potential response will be attained only if $f_{G,\text{micro}}$, defined as

$$f_{G,\text{micro}} = [f_G(t, q_G)]_{q_G \ll \sqrt{\pi Dt}} \quad (2.163)$$

reaches a constant value. The expressions for $f_{G,\text{micro}}$ corresponding to microhemispheres, microdiscs, microcylinders, and microbands are given in Table 2.3. The condition $f_{G,\text{micro}} = \text{constant}$ is only attained at disc and hemispherical electrodes (see Table 2.3). In both cases, the function $f_G(t, q_G)$ becomes independent of time when $q_G \ll \sqrt{\pi Dt}$.

For a spherical electrode, by making $r_s \ll \sqrt{\pi D_O t}$ in Eq. (2.137) (which has been deduced for unequal diffusion coefficients), and considering that both species are soluble in the electrolytic solution (upper sign), one obtains

$$I^{\text{microsphere, ss}} = FA_s D \frac{c_O^* - c_O^{r,s}}{r_s} = FA_s D \frac{c_O^* - e^\eta c_R^*}{1 + \gamma^2 e^\eta} \frac{1}{r_s} \quad (2.164)$$

or

$$E = E_{1/2}^{r,\text{micro}} + \frac{RT}{F} \ln \left(\frac{I_{d,c}^{\text{microsphere, ss}} - I}{I - I_{d,a}^{\text{microsphere, ss}}} \right) \quad (2.165)$$

where $c_O^{r,s}$ is given by Eq. (C.11) and

$$\left. \begin{aligned} I_{d,c}^{\text{microsphere, ss}} &= FA_s D_O c_O^* \frac{1}{r_s} \\ I_{d,a}^{\text{microsphere, ss}} &= -FA_s D_R c_R^* \frac{1}{r_s} \end{aligned} \right\} \quad (2.166)$$

The reversible half-wave potential is given by

$$E_{1/2}^{r, \text{microsphere}} = E_c^{\ominus'} + \frac{RT}{F} \ln \left(\frac{1}{\gamma^2} \right) \quad (2.167)$$

with $E_{1/2}^{r, \text{microsphere}}$ being the half-wave potential deduced for a microsphere or microhemisphere. As can be expected, the expression for $I_{d,c}^{\text{microsphere,ss}}$ given by Eq. (2.166) coincides with that of $I_{d,c}^{\text{sphere,ss}}$ for a spherical electrode given by Eq. (2.148).

In the case of an ultramicrodisc, the above equations become

$$\left. \begin{aligned} I_{d,c}^{\text{microdisc,ss}} &= 4Fr_d D_O c_O^* \\ I_{d,a}^{\text{microdisc,ss}} &= -4Fr_d D_R c_R^* \end{aligned} \right\} \quad (2.168)$$

It has been verified numerically that, when $D_O \neq D_R$, the stationary current-potential response of a microdisc presents the same half wave potential as that observed for a microsphere, which is given by Eq. (2.167) (see [70] and Appendix C).

Therefore, the stationary I - E response can be written as (Table 2.3)

$$I^{\text{microdisc,ss}} = FA_d D_O \frac{c_O^* - c_O^{r,s}}{r_d} \frac{4}{\pi} = FA_d D_O \frac{c_O^* - e^\eta c_R^*}{1 + \gamma^2 e^\eta} \frac{4}{\pi r_d} \quad (2.169)$$

where $c_O^{r,s}$ is given by Eq. (C.20).

The current densities ($i = I/A$) obtained for disc and microspheres of the same radius for reversible electrode processes at any value of the applied potential follow the equivalence relationship given by [70, 71]:

$$\frac{i^{\text{microdisc,ss}}}{i^{\text{microsphere,ss}}} = \frac{4}{\pi} \quad (2.170)$$

In the case of microcylinders and microbands, $f_{G,\text{micro}}$ is time dependent (Table 2.3) and only a pseudo-stationary response can be achieved. This is because all the microelectrode dimensions have to fall in the range of the microns to attain a true steady state. The expressions for the pseudo-stationary current-potential responses when the diffusion coefficients of species O and R fulfills $D_O = D_R$ are:

$$I^{\text{microcylinder, pss}} = FA_c D \frac{c_O^* - e^\eta c_R^*}{1 + e^\eta} \frac{1}{r_c} \frac{2}{\ln \left[\frac{4Dt}{r_c^2} \right]} \quad (2.171)$$

$$I^{\text{microband, pss}} = FA_b D \frac{c_O^* - e^\eta c_R^*}{1 + e^\eta} \frac{1}{w} \frac{2\pi}{\ln \left[\frac{64Dt}{w^2} \right]} \quad (2.172)$$

Nevertheless, it is possible to obtain a constant relationship between the current at both microelectrodes for certain geometrical conditions. Thus, for microbands and microhemicylinders fulfilling $r_c = w/4$, a constant ratio is obtained, but in this case it is necessary to use the same experimental timescale [10]:

$$\frac{I^{\text{microband, pss}}}{I^{\text{microhemicylinder, pss}}} = 1 \quad (2.173)$$

The solutions of the stationary diffusion equations for spherical and disc microelectrodes are deduced in Appendix C.

It is also of interest to consider the case of a microsphere at a non-electroactive substrate because it is used as a model for spherical nanoparticles (of radius r_{np} and area A_{np}) impacting on a surface [72, 73]. For this case the average stationary current is given by [74]:

$$I^{\text{np,ss}} = A_{\text{np}} D F \frac{c_{\text{O}}^* - c_{\text{O}}^{\text{r,s}}}{r_{\text{np}}} \ln 2 \quad (2.174)$$

Note that, on the basis of Eqs. (2.164), (2.169), and (2.174), it can be concluded that for all these electrode geometries for which it is possible to achieve a true stationary response, Eq. (2.165) could be used by changing $I_{\text{d,c}}^{\text{microsphere,ss}}$ by the corresponding stationary limiting current for the geometry considered. Therefore, in all the previous cases it is fulfilled,

$$E = E_{1/2}^{\text{r,microG}} + \frac{RT}{F} \ln \left(\frac{I_{\text{d,c}}^{\text{microG}} - I^{\text{microG}}}{I^{\text{microG}} - I_{\text{d,a}}^{\text{microG}}} \right) \quad (2.175)$$

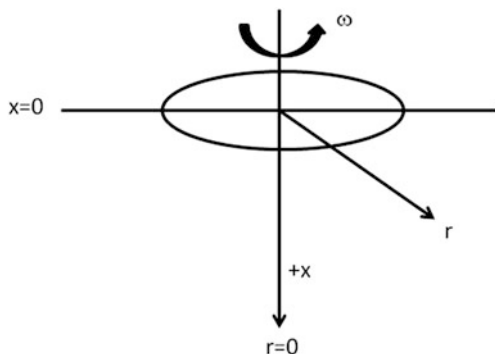
The advantages derived from the use of microelectrodes will be discussed in Sect. 5.4.

2.8 Rotating Disc Electrode

A rotating disc electrode (RDE) is a conductive disc of the material of interest embedded in an inert non-conductive polymer or resin that can be attached to an electric motor which has very fine control of the electrode's rotation rate. During the experiment, the electrode rotates in the solution under study, thus inducing a flux of redox analyte to the electrode [75].

The modeling of the electrochemical response corresponding to the application of a constant potential to an RDE is similar to that discussed in the case of a DME since in this electrode it is imperative to consider the convection caused by the rotation of the electrode. This problem was solved by Levich under stationary conditions [76]. To do this, the starting point is the diffusive-convective differential

Fig. 2.22 Polar coordinates for the rotating disc electrode



equation that describes the mass transport in the normal direction to the electrode surface (see Fig. 2.22),

$$\frac{\partial c_i}{\partial t} = D_i \frac{\partial^2 c_i}{\partial x^2} - v_x \frac{\partial c_i}{\partial x} \quad i = O, R \quad (2.176)$$

The convection velocity for an RDE is given by the following expression:

$$v_x = -0.51\omega^{3/2}\nu^{-1/2}x^2 \quad (2.177)$$

in which ω is the angular rotation speed (in Hz) and ν the kinematic viscosity (in $\text{m}^2 \text{s}^{-1}$).

Under steady-state conditions, i.e., when $\partial c_i / \partial t = 0$, Eq. (2.176) simplifies to

$$\left. \begin{aligned} \frac{d^2 c_i}{dx^2} &= -\frac{x^2}{B} \frac{dc_i}{dx} \quad i = O, R \\ B &= \frac{D_i}{0.51\omega^{3/2}\nu^{-1/2}} \end{aligned} \right\} \quad (2.178)$$

By making the change of variable $y = dc_i/dx$, Eq. (2.178) is easily integrated and the following expression is obtained:

$$\frac{dc_i}{dx} = \left(\frac{dc_i}{dx} \right)_{x=0} e^{-\frac{x^2}{3B}} \quad i = O, R \quad (2.179)$$

Integrating once more, the concentration profile,

$$c_i(x) - c_i(0) = \left(\frac{dc_i}{dx} \right)_{x=0} \int_0^x e^{-\frac{u^2}{3B}} du \quad i = O, R \quad (2.180)$$

By taking the infinite limit ($x \rightarrow \infty$) in the above equation, it becomes

$$\begin{aligned} c_i^* - c_i(0) &= \left(\frac{dc_i}{dx}\right)_{x=0} \int_0^{\infty} e^{-\frac{u^2}{3B}} du = \\ &= \left(\frac{dc_i}{dx}\right)_{x=0} (3B)^{1/3} \Gamma(3/4) = 1.29B^{1/3} \left(\frac{dc_i}{dx}\right)_{x=0} \end{aligned} \quad (2.181)$$

with $\Gamma(x)$ being the Euler Gamma function. By combining Eqs. (2.180) and (2.181) the following expression for the concentration profile is deduced:

$$c_i(x) - c_i(0) = \frac{c_i^* - c_i(0)}{1.29B^{1/3}} \int_0^x e^{-u^3/3B} du \quad i = O, R \quad (2.182)$$

Moreover, the current is given by

$$\begin{aligned} I^{\text{RDE}} &= FAD_O \left(\frac{dc_O}{dx}\right)_{x=0} = \frac{c_O^* - c_O(0)}{1.29B^{1/3}} = \\ &= 0.620FAD_O^{2/3} \omega^{1/2} \nu^{-1/6} (c_O^* - c_O(0)) \end{aligned} \quad (2.183)$$

which simplifies to the well-known Levich's equation for limiting conditions (i.e., $c_O(0) = 0$):

$$I_{d,c}^{\text{RDE}} = 0.620FAD_O^{2/3} \omega^{1/2} \nu^{-1/6} c_O^* \quad (2.184)$$

From Eqs. (2.183) and (2.184), it is possible to rewrite the expression of the surface concentrations in terms of the current, and the cathodic and anodic limiting currents are as follows:

$$\left. \begin{aligned} \frac{c_O(0)}{c_O^*} &= 1 - \frac{I^{\text{RDE}}}{I_{d,c}^{\text{RDE}}} \\ \frac{c_R(0)}{c_R^*} &= 1 - \frac{I^{\text{RDE}}}{I_{d,a}^{\text{RDE}}} \end{aligned} \right\} \quad (2.185)$$

with $I_{d,a}^{\text{RDE}}$ being identical to that given in Eq. (2.184) by changing D_O and c_O^* by D_R and c_R^* and of negative sign. By combining Eq. (2.185) with the nernstian condition $e^\eta = c_O(0)/c_R(0)$, with η given by Eq. (2.6), the following relationship between current and potential is given by

$$E = E_{1/2}^{\text{r,RDE}} + \frac{RT}{F} \ln \left(\frac{I_{d,c}^{\text{RDE}} - I^{\text{RDE}}}{I^{\text{RDE}} - I_{d,a}^{\text{RDE}}} \right) \quad (2.186)$$

which is formally identical to that obtained at planar electrodes (Eq. 2.31), but the half-wave potential is

$$E_{1/2}^{\text{r,RDE}} = E_c^{\ominus'} + \frac{RT}{F} \ln \left(\frac{D_R}{D_O} \right)^{2/3} \quad (2.187)$$

2.9 Thin Layer Voltammetry

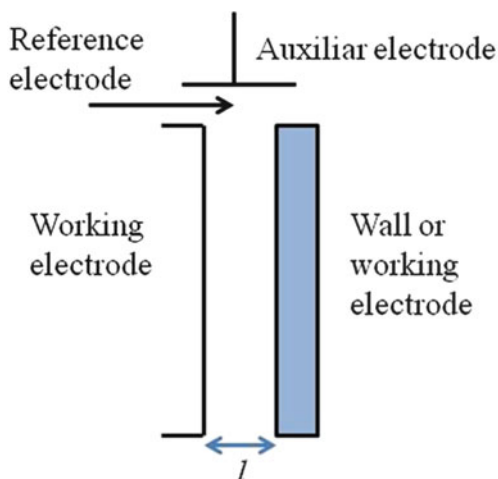
This section analyzes the response of a charge transfer process under conditions of finite linear diffusion which corresponds to a thin layer cell. This type of cell can be achieved by miniaturization process for obtaining a very high Area/Volume ratio, i.e., a maximum distance between the working and counter electrodes that is even smaller than the diffusion layer [31]. In these cells it is easy to carry out a bulk electrolysis of the electroactive species even with no convection. Two different cell configurations can be described: a cell with two working electrodes or a working electrode versus an electro-inactive wall separated at distance l (see Fig. 2.23).

If we consider a thin layer cell where the electrode process given in reaction Scheme (I) takes place, the mass transport differential equation is given by Eq. (2.2) and the boundary conditions corresponding to limiting current are as follows:

$$t = 0, 0 \leq x \leq l \quad c_O = c_O^*, c_R = 0 \quad (2.188)$$

$$t > 0$$

Fig. 2.23 Diagram of a thin layer cell with a single or two working electrodes



$$\left. \begin{aligned} c_O(0, t) = c_O(l, t) = 0 \\ \left(\frac{\partial c_O}{\partial x} \right)_{x=l/2} = 0 \end{aligned} \right\} \text{two working electrodes} \quad (2.189)$$

$$\left. \begin{aligned} c_O(0, t) = 0 \\ \left(\frac{\partial c_O}{\partial x} \right)_{x=l} = 0 \end{aligned} \right\} \text{one working electrode} \quad (2.190)$$

The solution to Eq. (2.2) can be deduced by using Laplace transform method (see Appendix B), by obtaining the following expression:

$$\bar{c}_O(x, p) = \frac{c_O(x, 0)}{p} + a_1 e^{\sqrt{\frac{p}{D_O}}x} + a_2 e^{-\sqrt{\frac{p}{D_O}}x} \quad (2.191)$$

In order to determine the values of constants a_1 and a_2 , the derivative of Eq. (2.191) is equated to zero at the corresponding distance ($x = l/2$ or $x = l$) in line with Eqs. (2.189) and (2.190):

$$a_1 e^{\sqrt{\frac{p}{D_O}}\delta} - a_2 e^{-\sqrt{\frac{p}{D_O}}\delta} = 0 \quad (2.192)$$

where $\delta = l/2$ for the two electrodes cell and $\delta = l$ for the one electrode cell. By combining Eq. (2.192) and condition $\bar{c}_O(0, p) = 0$, one obtains

$$a_1 = \frac{-c_O^*}{p} \frac{e^{-\sqrt{\frac{p}{D_O}}\delta}}{e^{\sqrt{\frac{p}{D_O}}\delta} + e^{-\sqrt{\frac{p}{D_O}}\delta}} \quad (2.193)$$

$$a_2 = \frac{-c_O^*}{p} \frac{e^{\sqrt{\frac{p}{D_O}}\delta}}{e^{\sqrt{\frac{p}{D_O}}\delta} + e^{-\sqrt{\frac{p}{D_O}}\delta}} \quad (2.194)$$

The Laplace transform of the current is given by

$$\bar{I}^{\text{TLV}}(p) = FAD_O \left(\frac{\partial \bar{c}_O}{\partial x} \right)_{x=0} = FAD_O \sqrt{\frac{p}{D_O}} [a_1 - a_2] \quad (2.195)$$

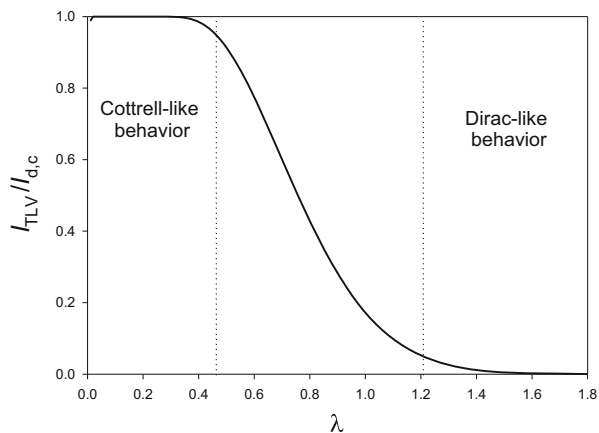
which, by taking into account Eqs. (2.193) and (2.194), becomes [31]:

$$\bar{I}^{\text{TLV}}(p) = FAc_O^* \sqrt{\frac{D_O}{p}} \frac{e^{\sqrt{\frac{p}{D_O}}\delta} - e^{-\sqrt{\frac{p}{D_O}}\delta}}{e^{\sqrt{\frac{p}{D_O}}\delta} + e^{-\sqrt{\frac{p}{D_O}}\delta}} = FA \sqrt{\frac{D_O}{p}} \tanh \left(\sqrt{\frac{p}{D_O}}\delta \right) \quad (2.196)$$

As indicated in reference [77] the inverse transform of Eq. (2.196) leads to

$$\frac{I^{\text{TLV}}}{I_{d,c}} = 4\lambda \sum_{m=1}^{\infty} \exp \left[-(2m-1)^2 \pi \lambda^2 \right] \quad (2.197)$$

Fig. 2.24 Variation of the ratio ($I_{\text{TLV}}/I_{\text{d,c}}$) versus λ calculated from Eq. (2.197)



with

$$\lambda = \begin{cases} \frac{\sqrt{\pi D_{\text{O}} t}}{l} & \text{two working electrodes} \\ \frac{\sqrt{\pi D_{\text{O}} t}}{2l} & \text{one working electrode} \end{cases} \quad (2.198)$$

and $I_{\text{d,c}}$ being the diffusion-controlled limiting current (see Eq. 2.28). Equation (2.197) simplifies in two asymptotic cases. When $\lambda \rightarrow 0$ (i.e., $l \gg \sqrt{\pi D_{\text{O}} t}$), the term $4\lambda \sum_{m=1}^{\infty} \exp[-(2m-1)^2 \pi \lambda^2] \rightarrow 1$ in such a way the current becomes identical to $I_{\text{d,c}}$ (that is, the expression corresponding to the semi-infinite approach). In the contrary, i.e., for $\lambda \rightarrow \infty$ (and $l \ll \sqrt{\pi D_{\text{O}} t}$), the current expression simplifies to [31],

$$I_{\lambda \rightarrow \infty}^{\text{TLV}} = FAc_{\text{O}}^* l \times \text{Dirac}(t) \quad (2.199)$$

This result indicates that as l decreases the current takes a very high value at times close to zero and it diminishes very fast (i.e., species O is consumed instantaneously). In order to check the values of parameter λ for which the response evolves from the cottrellian behavior to that given by Eq. (2.199), the behavior of the ratio ($I^{\text{TLV}}/I_{\text{d,c}}$) versus λ has been plotted in Fig. 2.24. From this figure, it can be seen that for $\lambda \leq 0.46$ the current is identical to that obtained with the Cottrell equation (with a maximum relative difference of 5 %). For higher values of λ , the ratio decreases until for $\lambda \geq 1.21$ the current behaves in line with Eq. (2.199) (with a maximum relative difference of 5 %). In practice, that means that the current will be similar to that obtained at a “semi-infinite” cell for times close to zero and it will decrease with time faster, the smaller the value of l (i.e., the faster λ increases) due

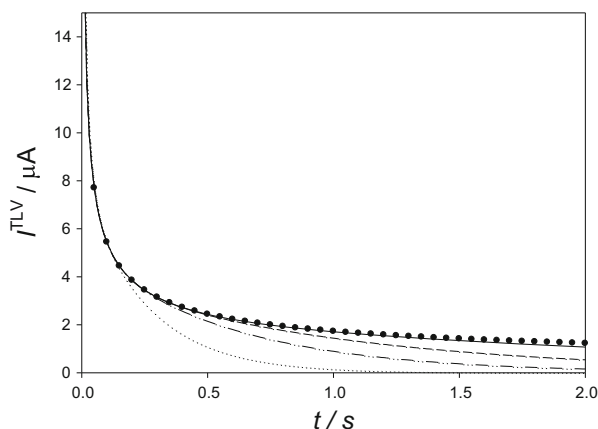


Fig. 2.25 Chronoamperometric responses of a thin layer cell calculated from Eq. (2.197) for different values of l (in μm): 150 (solid line); 100 (dashed line); 75 (dashed-dotted line); and 50 (dotted line). The current calculated with Cottrell Eq. (2.28) is also plotted (black dots). $D = 10^{-5} \text{ cm}^2 \text{ s}^{-1}$, $A = 0.01 \text{ cm}^2$, $c_0^* = 10^{-6} \text{ mol cm}^{-3}$

to a faster depletion of the oxidized species, which can be seen in Fig. 2.25. For example, for a fixed time of one second, the current obtained for a separation between electrodes of $150 \mu\text{m}$ is undistinguishable from that obtained under semi-infinite linear diffusion whereas it drops 48 % from the cottrellian value when the distance is $l = 75 \mu\text{m}$. This decrease reaches 91 % for the narrower cell ($l = 50 \mu\text{m}$), for which, at this time, the current is very close to zero.

References

1. Galus Z (1993) Fundamentals of electrochemical analysis, 2nd/rev edn. Ellis Horwood series in analytical chemistry. Ellis Horwood, Chichester
2. Bard AJ, Faulkner LR (2001) Electrochemical methods, fundamental and applications. Wiley, New York, NY
3. Heyrovský J (1966) Principles of polarography. Academic, New York, NY
4. MacDonald DD (1958) Transient techniques in electrochemistry. Plenum, New York, NY
5. Barker GC (1958) Anal Chim Acta 18:118–131
6. Barker GC, Gardner AW (1958) Atomic Energy Res Estab Harwell C/R 2297
7. Barker GC, Gardner AW (1960) Z Anal Chem 173:79–83
8. Bard AJ, Inzelt G, Scholz F (eds) (2008) Electrochemical dictionary. Springer, Berlin
9. Montenegro I, Queiros MA, Daschbach JL (eds) (1991) Microelectrodes: theory and applications (Nato Science Series E). Kluwer Academic, Dordrecht
10. Amatore C (1995) In: Rubinstein I (ed) Physical electrochemistry: principles, methods and applications. Marcel Dekker, New York, NY
11. Brett CMA, Brett AMO (1993) Electrochemistry: principles, methods, and applications. Oxford University Press, Oxford

12. Molina A, Gonzalez J, Martinez-Ortiz F, Compton RG (2010) *J Phys Chem C* 114:4093–4099
13. Cottrell FG (1902) *Z Phys Chem* 42:385
14. Gao X, Lee J, White HS (1995) *Anal Chem* 67:1541–15445
15. Amatore C, Knobloch K, Thouin L (2007) *J Electroanal Chem* 601:17–28
16. Amatore C, Pebay C, Thouin L, Wang A (2009) *Electrochem Commun* 11:1269–1272
17. Tomeš J (1937) *Czech Collect Chem Commun* 9:12
18. Koryta J, Vanýsek P, Brezina M (1977) *J Electroanal Chem* 75:211–228
19. Samec Z (2004) *Pure Appl Chem* 76:2147–2180
20. Volkov AG (1988) *Electrochim Acta* 44:139–153
21. Peljo P, Murtomäki L, Kallio T, Xu HJ, Meyer M, Gros CP, Barbe JM, Girault HH, Laasonen K, Kontturi KS (2012) *J Am Chem Soc* 134:5974–5984
22. Molina A, Serna C, Ortuño JA, Torralba E (2012) *Annu Rep Prog Chem Sect C* 108:126–176
23. Gavach C, Młodnicka T, Guastalla J (1968) *C R Acad Sci C* 266:1196–1199
24. Vanýsek P (1995) *Electrochim Acta* 40:2841–2847
25. Shirai O, Kihara S, Yoshida Y, Matsui M (1995) *J Electroanal Chem* 389:61–70
26. Langmaier J, Samec Z (2007) *Electrochem Commun* 9:2633–2638
27. Senda M, Kakiuchi T, Osakai T (1991) *Electrochim Acta* 36:253–262
28. Scholz F (2006) *Annu Rep Prog Chem Sect C* 102:43–70
29. Ortuño J, Serna C, Molina A, Torralba E (2009) *Electroanalysis* 21:2297–2302
30. Molina A, Serna C, Gonzalez J, Ortuño J, Torralba E (2009) *Phys Chem Chem Phys* 11: 1159–1166
31. Girault HH (2004) *Analytical and physical electrochemistry, Fundamental sciences series*. EFPL Press, Lausanne
32. Ilkovič D (1934) *Czech Collect Chem Commun* 6:498–513
33. Kolthoff IM, Lingane JJ (1952) *Polarography*, 2nd edn. Wiley-Interscience, New York, NY
34. Meites L (1958) *Polarographic techniques*, 2nd edn. Wiley-Interscience, New York, NY
35. Koutecký J (1953) *Czech J Phys* 2:50–58
36. Koutecký J, Stackelberg MV (1962) In: Zuman P, Kolthoff IM (eds) *Progress in polarography*, vol I. Wiley-Interscience, New York, NY
37. Newman J (1967) *J Electroanal Chem* 15:309–312
38. Brikmann AAAM, Loss JM (1964) *J Electroanal Chem* 7:171–183
39. Galvez J, Serna A (1976) *J Electroanal Chem* 69:133–143
40. Molina A, Serna C, Camacho L (1995) *J Electroanal Chem* 394:1–6
41. Molina A, Serna C (1999) *J Electroanal Chem* 466:8–14
42. Wang J (2006) *Analytical Electrochemistry*, 3rd edn. Wiley-VCH, New York, NY
43. Lovrić M (2002) *Stripping voltammetry*. In: Scholz F (ed) *Electroanalytical methods: guide to experiments and applications*. Springer, Berlin
44. Demaille C, Brust M, Tsionsky M, Bard AJ (1997) *Anal Chem* 69:2323–2328
45. Amatore C, Maisonhaute E, Schöllhorn B, Wadhawan J (2007) *Chem Phys Chem* 8: 1321–1329
46. Martinez Ortiz F, Laborda E, Limon-Petersen JG, Rogers EI, Serna C, Rees NV, Molina A, Compton RG (2009) *J Phys Chem C* 113:17215–17222
47. Scholz F (2011) *J Solid Stat Electrochem* 15:1699–1702
48. Hapiot P, Lagrost C (2008) *Chem Rev* 108:2238–2264
49. Molina A, Laborda E, Rogers EI, Martinez-Ortiz F, Serna C, Limon-Petersen JG, Rees NV, Compton RG (2009) *J Electroanal Chem* 634:90–97
50. Rogers EI, Silvester DS, Poole DL, Aldous L, Hardacre C, Compton RG (2008) *J Phys Chem C* 112:2729–2735
51. Laborda E, Rogers EI, Martinez-Ortiz F, Limon-Petersen JG, Rees NV, Molina A, Compton RG (2009) *J Electroanal Chem* 634:1–10
52. Molina A, Serna C, Martínez-Ortiz F, Laborda E (2008) *J Electroanal Chem* 617:14–26
53. Delmastro JR, Smith DE (1966) *Anal Chem* 38:169–179
54. Delmastro JR, Smith DE (1967) *J Phys Chem* 71:2138–2149

55. MacGillavry D, Rideal EK (1937) *Recl Trav Chim* 56:1013
56. Polo S, Llopis J, Rius A (1949) *An Quim* 45:1029
57. Saito Y (1968) *Rev Polarograph* 15:177–187
58. Compton RG, Banks CE (2011) *Understanding voltammetry*, 2nd edn. ICP, London
59. Molina A, Gonzalez J, Henstridge M, Compton RG (2011) *Electrochim Acta* 56:4589–4594
60. Molina A, Gonzalez J, Henstridge M, Compton RG (2011) *J Phys Chem C* 115:4054–4062
61. Alden JA, Hutchinson F, Compton RG (1997) *J Phys Chem B* 101:949–958
62. Rees NV, Zhou YG, Compton RG (2012) *RSC Adv* 2:379–384
63. Kwon SJ, Fu-Ren F, Bard AJ (2010) *J Am Chem Soc* 132:13165–13167
64. Hellberg D, Scholz F, Schauer F, Weitschies W (2002) *Electrochem Commun* 4:305–309
65. Hellberg D, Scholz F, Schubert F, Lovrić M, Omanović D, Hernandez VA, Thede R (2005) *J Phys Chem B* 109:14715–14726
66. Forster RJ (2003) Microelectrodes: retrospect and prospect. In: Bard AJ, Stratmann M, Unwin P (eds) *Encyclopedia of electrochemistry*, vol 3, Instrumentation and electroanalytical chemistry. Wiley-VCH, Weinheim, pp 160–195
67. Zoski CG (ed) (2007) *Handbook of electrochemistry*. Elsevier, Amsterdam
68. Wang Y, Velmurugan J, Mirkin MV (2010) *Isr J Chem* 50:291–305
69. Wightman RM, Wipf DO (1988) Voltammetry at Ultramicroelectrodes. In: Bard AJ (ed) *Electroanalytical chemistry*, vol 15. Marcel Dekker, New York, pp 267–353
70. Oldham KB, Zoski CG (1988) *J Electroanal Chem* 256:11–19
71. Amatore CA, Fosset B (1992) *J Electroanal Chem* 328:21–32
72. Henstridge M, Compton RG (2012) *Chem Rec* 12:63–71
73. Bobbert PA, Winf MM, Vlieger J (1987) *Phys A* 141:58–72
74. Molina A, Gonzalez J, Barnes EO, Compton RG (2014) *J Phys Chem C* 118:346–356
75. Newman JS (1991) *Electrochemical Systems*, 2nd edn. Prentice Hall, Englewood Cliffs, NJ, Chaps. 15 and 17
76. Levich VG (1962) *Physicochemical hydrodynamics*. Prentice-Hall, Englewood Cliffs, NJ
77. Hubbard AT, Anson FC (1970) The theory and practice of electrochemistry with thin layer cells. In: Bard AJ (ed) *Electroanalytical chemistry*, vol 4. Marcel Dekker, New York, NY, pp 129–214

Pulse Voltammetry in Physical Electrochemistry and
Electroanalysis

Theory and Applications

Molina, Á.; González, J.

2016, XV, 671 p., Hardcover

ISBN: 978-3-319-21250-0